International Journal of Greenhouse Gas Control 113 (2022) 103521

Contents lists available at ScienceDirect

International Journal of Greenhouse Gas Control

journal homepage: www.elsevier.com/locate/ijggc

A part-load analysis and control strategies for the Graz Cycle

Benjamin Mitterrutzner [a,b,c], Wolfgang Sanz [*,a], Lars O. Nord [b]

[a] Institute for Thermal Turbomachinery and Machine Dynamics, Graz University of Technology, Graz, Austria
[b] Department of Energy and Process Engineering, Norwegian University of Science and Technology, Trondheim, Norway
[c] Energy, Climate, and Environment Program, International Institute for Applied Systems Analysis, Laxenburg, Austria

ARTICLE INFO

Keywords:
Graz Cycle
Oxy-combustion cycle
Plantwide control strategy
Optimal part-load operation
Off-design modelling and simulation
Carbon capture and storage

ABSTRACT

Carbon capture and storage (CCS) plays a uniquely important role in the future clean and dispatchable power generation portfolio to achieve the ambitious goals set at COP21. The Graz Cycle, a zero emission oxy-combustion power plant, is one of the most promising representatives of CCS power generation plants. The present work introduces different control strategies for the Graz Cycle and the corresponding part-load performances. The process simulation is composed of a design-point (full-load) and off-design (part-load) of the cycle. In order to do this, the process simulation tool IPSEpro was used. Individual cycle components were modelled for both investigations, full load and part load, and control strategies were developed in order to achieve optimum performances and operating efficiencies by means of the assumptions given. This work distinguishes from previous studies by the development of different control strategies and comparison of corresponding part-load performances. In the simulation, the Graz Cycle operating at nominal design conditions achieved a net plant efficiency of 53.1%. The part-load simulation generated results down to 40% load by applying three different control strategies. These control operation modes differ from each other in two basic parameters, boiler pressure and turbine inlet temperature. Optimum part-load performances were achieved by control strategy, where the pressure of the heat recovery steam generator is allowed to vary. However, other parameters, e.g. costs, did not appear to be favourable for this operation mode. The comparison with a readily available technology, such as a natural gas combined cycle, showed that the Graz Cycle is more efficient as loads are reduced below 50%.

1. Introduction

The average earth surface temperature has risen by 0.8 °C since the industrial revolution as a result of the increased atmospheric concentration of greenhouse gases (primarily CO_2) due to anthropogenic activities (Fischedick et al., 2015). In light of the commitments agreed on COP21, the temperature increase must not exceed the 1.5–2 °C temperature level in order to limit the consequences of climate warming in ecosystems (Bui et al., 2018). These challenges will primarily concern the electricity and heat generating sector, which produces the lion's share of man-made greenhouse gas emissions (Center for Climate and Energy Solutions, 2017; European Commission, 2011; IEA, 2020). Besides strong support measures for renewable energy sources, the European Union confirmed that Europe cannot be decarbonised cost-efficiently without a significant support of carbon capture and storage (CCS) (Zero Emissions Platform, 2013). Thus, CCS is a key technology for fossil fuel based power generation, that reduces directly CO_2 emissions at large scale and provides stability and balancing capacity to the power supply system (Littlecott et al., 2014). Integrating fluctuating renewables into the future power grid and at the same time providing sustainable electricity supply is complex, since supply and demand are linked physically and an increase or decrease of one part has to be balanced instantly by the other (IEA, 2011). Hence, the whole power system and every unit of the electricity supply pool has to operate dynamically to overcome the intermittent nature of renewables, which demands high flexibility of power plants in order to do load changes and part-load operation (Johnsson et al., 2013). In this context lays the utterly importance of this study.

Three main methodologies for CO_2 capture from combustion of fossil fuels exist (Koohestanian and Shahraki, 2021; Mitterrutzner, 2020; Zheng, 2011):

(i) Conventional power cycles with CO_2 removal from the waste gas (post-combustion capture)
(ii) CO_2 separation from the fuel and combustion of pure H_2 in a power plant (pre-combustion capture)

* Corresponding author.
E-mail address: wolfgang.sanz@tugraz.at (W. Sanz).

https://doi.org/10.1016/j.ijggc.2021.103521
Received 1 June 2021; Received in revised form 5 October 2021; Accepted 11 November 2021
Available online 30 November 2021
1750-5836/© 2021 The Author(s). Published by Elsevier Ltd. This is an open access article under the CC BY license (http://creativecommons.org/licenses/by/4.0/).

Nomenclature

HTT	high temperature turbine
LPT	low pressure turbine
HPT	high pressure turbine
LPST	low pressure steam turbine
C	compressor
ECO	economizer
IC	intercooler
SH	superheater
GC	Graz Cycle
NG	natural gas
NGCC	natural gas combined cycle
OTSG	once-through steam generator
VIGV	variable inlet guide vane
V	valve
P	power
LHV	lower heating value
MV	manipulated variable
CV	controlled variable
TIT	turbine inlet temperature
TET	turbine exhaust temperature
CPU	compression and purification unit
ASU	air separation unit
CCS	carbon capture and storage
DOF	control degree of freedom
λ	excess air ratio [–]
μ	mass fraction [kg/kg]
π	pressure ratio [bar/bar]
η	efficiency [%]
ω	rotational speed [min^{-1}]
Φ	relative value [–]
Δ	difference [–]
p	pressure [bar]
k	heat transfer coefficient [W/m^2 K]
A	area [m^2]
R	gas constant [J/kmolK]
t	temperature [°C]
T	temperature [K]
n	polytropic coefficient [–]
St	Stanton number [–]
n	turbine speed [Hz]
x	vapour quality [kg/kg]
c	specific heat capacity [kJ/(kg K)]
h	enthalpy [kJ]
$\dot{m}$	mass flow rate [kg/s]
F	mass flow rate [kg/s]
$\dot{W}$	mechanical power generation [MW]
0	design point value
α	steam turbine inlet section
ω	steam turbine outlet section
s	steam
a	uncooled
s	isentropic process
f	feed condition
feed	feed condition
drain	drain condition
3	turbine inlet section
4	turbine outlet section
1	compressor inlet section
2	compressor outlet section
h	hot-side heat exchanger
p	constant pressure condition
T	turbine
C	compressor
out	total output value
in	total input value
min	minimum value
max	maximum value
e	exiting stream condition
sp	set point

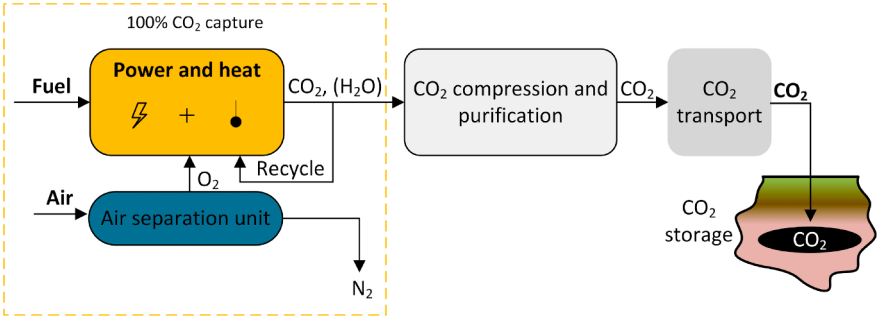

Fig. 1. Operating principle of an oxy-combustion capture process.

(iii) Combustion with pure oxygen (produced by an air separation unit), which leads to a flue gas consisting of CO_2 and water with condensation of latter to obtain pure CO_2 (oxy-combustion capture)

The process we study herein is based on methodology (iii) above. The Graz Cycle (described in more detail in Section 2.1) is an advantageous representative of oxy-combustion concepts with a theoretical capture rate of 100% (IEAGHG, 2015; Sanz et al., 2005). The fundamental idea of an oxy-combustion power plant is producing clean energy by avoiding the dilution of combustion products with nitrogen. In order to achieve that, the combustion takes place with pure or almost pure oxygen, producing a flue gas, which consists mainly out of CO_2 and H_2O. To attain a high efficiency, a big part of the exhaust gas is recycled to the combustor (Mitterrutzner, 2020). Oxy-combustion gas turbine power plants are generally "highly integrated, involving energy and mass recycle, and optimizing efficiency might lead to operational (control) challenges. Therefore it is important to look at the interplay between process design and control (Snarheim et al., 2005)". Thus, this study expands the work of past studies by an in-depth analysis of control

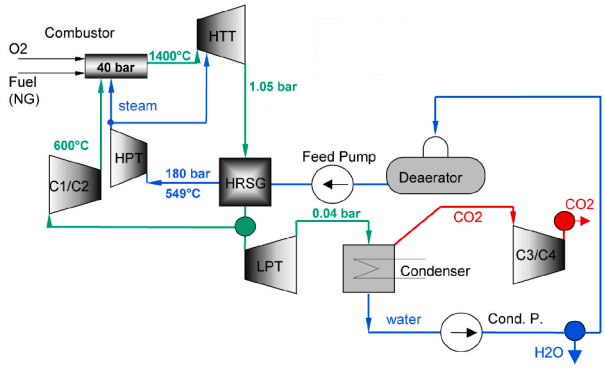

Fig. 2. Simplified flowsheet of the Basic Graz Cycle (based on Sanz et al., 2005). Water is in blue and cycle fluid in green and CO2 in red. (For interpretation of the references to colour in this figure legend, the reader is referred to the web version of this article.)

strategies applied to the Graz Cycle alongside a framework that identifies manipulated and controlled variables to finally achieve an optimal control scheme for the subjacent process. The goal is to find a control strategy - possibly a simple one - with ideal part-load efficiencies and thus optimal operational costs by maintaining important process parameters within its boundary conditions.

Fig. 1 illustrates the methodology of an oxy-combustion capture process within the CCS supply chain. It is composed by the (i) capturing process, which results in a waste gas mixture of mainly CO_2 and water vapor, the subsequent (ii) separation and (iii) purification process of the CO_2 stream by cooling and compressing the gas to a high density, (iv) CO_2 transport, e.g. *via* pipeline, and finally the (v) long-term carbon dioxide storage in suitable geographical formations like depleted oil and gas reservoirs, deep saline aquifers or coal beds (Metz et al., 2005).

The literature on part-load performance of the Graz Cycle is scarce, first investigations were done by Milewski et al. (2012); Miller et al. (2003) and Sanz et al. (2018), the latter two for a power cycle operated with pure hydrogen. Milewski et al. identified the two main routes to control the Graz Cycle *via* change on the working medium mass flow side (by compressor outlet mass flow rate) and change on the flow of the hydrogen-oxygen mixture supplied to the combustor (by fuel mass flow rate) Milewski et al. (2012). Sanz et al. revealed that the peak temperature (i.e. the turbine inlet temperature of the high temperature turbine) is - similar to combined cycles - crucial for the part-load efficiency of the oxy-combustion Graz Cycle. They managed to maintain reasonable process parameters at part loads through a slight decrease of the peak temperature down to 75% load. For further load reduction the control strategy was changed and the temperature dropped significantly in the same load interval. Part-load operation of the Graz Cycle down to 30% was shown to be feasible (Sanz et al., 2018).

The novelty of this work is the inclusion of plantwide control strategies alongside part-load performance analyses plus a systematic approach to achieve a control design for the underlying power cycle. To the authors best knowledge no such rigorous investigation has been done on any oxy-combustion cycle so far. Indeed, very few studies within CCS have a control focus. A similar procedure is done in the work by Zotică et al. (2019, 2020) for a simple steam heat-to-power cycle. Control design including modelling and simulation of a semi-closed gas turbine cycle for CO_2 capture is found in Snarheim et al. (2005) and Imsland et al. (2004). Zaryab et al. (2020) presented in their work control strategies for the oxy-combustion Allam Cycle and corresponding part-load results. They have developed different control strategies by variation of operational parameters of turbines (*via* partial arc admission schemes) and compressors (*via* variable inlet guide vanes and diffuser guide vanes schemes). Another important resource in the evaluation of control strategies for the oxy-combustion Graz Cycle is the similarity to control operation modes used in combined cycles. Existing state-of-the-art control methods for combined cycles are found in Gülen (2019); Kehlhofer et al. (1999) and Fan et al. (2021).

The study is organized as follows: in Chapter 2 the methods including the cycle description and the modelling is presented, the plantwide control strategies are described in Chapter 3, followed by the simulation results in Chapter 4 and the discussion with final remarks in Chapter 5. Appendix A discusses the integration of the Graz Cycle in the future power grid framework, whereas Appendix B shows the performance tables of the control strategies and the natural gas combined cycle.

2. Methods

This chapter presents methods and tools for the process simulation to ultimately achieve optimal control strategies for the Graz Cycle. First of all, the cycle arrangement is described, subsequently the process control methodology and the modelling is explained in detail by inclusion of assumptions, limitations and boundary conditions.

2.1. Cycle description

The reference cycle for this study is the Graz Cycle[1] presented by Sanz et al. (2005). A simplified process flow scheme of the cycle configuration is illustrated in Fig. 2 and key input data for the Graz Cycle are following[2]:

- Natural gas as a fuel input;
- Almost pure oxygen as a oxidant input, i.e. 95% O_2, 3.33% Ar, 1.66% N_2.

Natural gas (NG) is burned by the high purity oxygen at a pressure of 40 bar. Oxygen purity of 95% at the air separation unit (ASU) exit represents a good compromise between energy consumption (respectively cost expenditure) and cycle efficiency and thus is commonly used for oxy-combustion power plants (Darde et al., 2009; Lockwood, 2014; Prosser and Shah, 2011; Zheng, 2011). Steam and a recycled CO_2/H_2O mixture keep the turbine inlet temperature at constant levels (1400 °C) and cool the burners and the liner of the combustor. This is necessary since the theoretical combustion temperature of pure oxygen is about 3500 °C (Kehlhofer et al., 2009).

The exhaust gas consisting of water steam and CO_2 is then led to the high temperature turbine (HTT) and expanded to 1.05 bar and 569 °C. The cooling of the HTT is performed by splitting steam after the high pressure turbine (HPT), leading to a working fluid composition of 76% H_2O and 22% CO_2 at the HTT exit. After the turbine, the gas is cooled down in the heat recovery steam generator (HRSG) for vaporising and superheating steam directed to the HPT. Around 46% of the cycle mass flow gets subsequently forwarded to the LPT and expanded to the condenser pressure of 0.041 bar into the wet steam area by passing the water saturation line. The condenser is supplied with cooling water at a temperature of 10 °C, separating the liquid water content from the gaseous phase. Following, the gas is compressed by the compressors C3/C4 with an intermediate cooler for further extraction of condensed water. The CO_2 at the outlet has a purity of 90% at atmospheric pressure level (according to this investigation, that includes an additional cooler before the drain gas outlet). At this stage it enters the CPU, where it is purified and compressed to 100 bar, according to this study.

After the separation of liquid water in the condenser, it is forwarded

[1] The difference between the cycle layout of this study and the reference cycle is the addition of a cooler after the compressor C4 and a water feed from the water separator after compressor C3 to the condenser water drain stream. For a clear understanding refer to the overall process schemes of both.

[2] For component efficiencies and losses, alike the natural gas composition, Sanz et al. (2005) research is referred. Every deviation in efficiency or power consumption is noted in this present study.

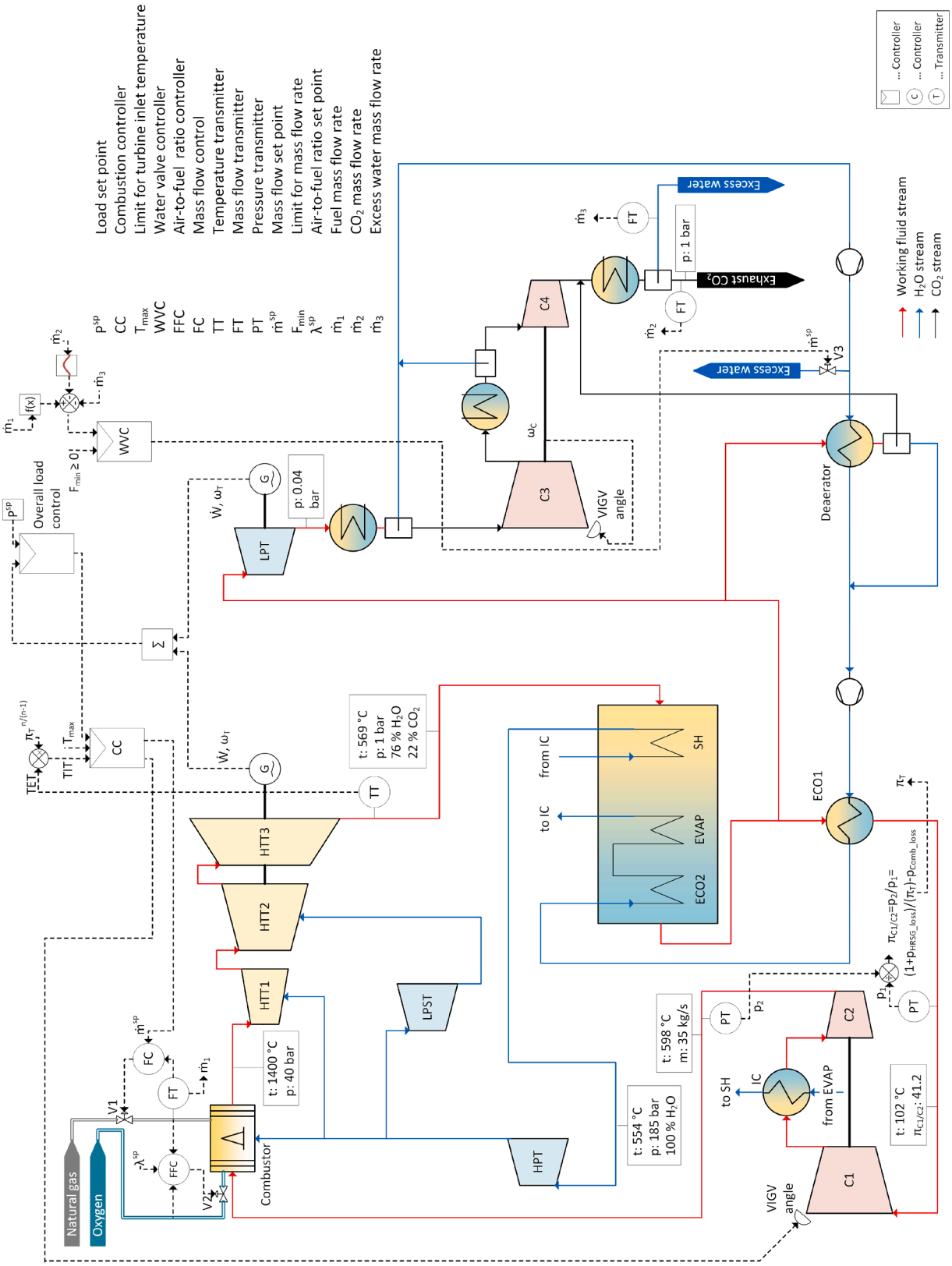

Fig. 3. Structure of the load control system of the Graz Cycle. Data is valid for nominal load (i.e. full-load) operation.

to the deaerator, whose heat is provided by a split stream of the hot flue gas after the HRSG (see Fig. 3). From there on the liquid H_2O is pre-heated in the following economizer, evaporated and finally superheated by the C1/C2 intercooler and the HRSG superheater to the HPT inlet conditions of 185 bar and 554 °C. The water steam after the expansion is used for cooling the combustor and the HTT turbine. After the HRSG, the major part of the working fluid is recycled to the combustor after being recompressed by an intercooled compressor C1/C2.

According to this study the net cycle efficiency of the Graz Cycle operating at base load is 53.1%. This value includes the energy

Table 1
Definition of CVs, MVs and DVs.

Variable name	Definition
CVs: controlled variables	
	• All those process variables that are controlled (i.e. active constraints);
	• they are referred to as the set points of the process (Seborg et al., 2008);
	• in a feedback control loop all CVs are measured (Seborg et al., 2008);
	• CVs contribute to the stabilization of the process, e.g. pressures (Zotică et al., 2020).
MVs: manipulated variables	
	• All those process variables that can be adjusted;
	• their goal is to keep CVs at their set point;
	• selection of MVs is equal to the identification of the steady-state control degrees of freedom (DOF) (Skogestad, 2004);
	• MVs are typically mass flow rates (Seborg et al., 2008).
DVs: disturbance variables	
	• All those process variables that affect CVs but cannot be adjusted, i.e. not manipulated input variables;
	• DVs are typically related to changing environment conditions, e.g. ambient temperatures, or a change in the natural gas composition (Seborg et al., 2008).

Table 2
Three different part-load control strategies for the Graz Cycle.

Strategy	Description, analysis	Pressure HRSG	TIT
S1	Within the power plant load rate from 100% to 40%: • TIT is not controlled actively but load-dependent; • condensing pressure is constant; • orifices fix the cooling streams for HTT; • usage of VIGVs.	p=1 bar	$t = t(\dot{W})$
S2	Within the power plant load rate from 100% to 55%: • TIT maintains the design value; • condensing pressure is constant; • throttle control for HTT1 cooling stream; • usage of VIGVs.	p=1 bar	$t = 1400\ ^{\circ}C$
S3	Within the power plant load rate from 100% to 40%: • TIT maintains the design value; • condensing pressure is constant; • throttle control for HTT1 cooling stream; • floating pressure control for LPT; • usage of VIGVs.	$p = p(\dot{W})$	$t = 1400\ ^{\circ}C$

consumption of oxygen supply and compression in the ASU and carbon dioxide compression to transport and storage conditions of 100 bar.

Table 4 shows the differences between the full-load performances (design conditions are set at 100% load) of Sanz et al. (2005) and this study. Both investigations show the same thermal cycle efficiency of 66.5%. Albeit the mechanical losses between the two analyses are kept the same, this study depicts a net electrical cycle efficiency advantage of 0.1%-points (i.e. 64.6% versus 64.7%). If considering the energy expenditure for oxygen production and compression to combustor inlet pressure level of 41.7 bar an efficiency of 55.3% compared to 54.8% results. This gain in efficiency stems from the production of the cycle oxidant with 95%-purity (instead of 100%-purity) which is much less energy expensive. In practice, the cryogenic O_2 -generation is valued 757 kJ/kg[3] (compared to 900 kJ/kg of the previous study). This change in values is due to techno-economical reasons. Furthermore, oxygen compression from 2.38 to 42 bar accounts for an energy expenditure of 325 kJ/kg (same value for both investigations).

For this study, the CO_2-compression value of 300 kJ/kg[3] (instead of 350 kJ/kg) for the compression from 1 to 100 bar is set as a new assumption. This results in a overall net efficiency of 53.3% against 52.6% of the Sanz et al. (2005) study.

2.2. Process control procedure

Power plants are usually operated in order to correspond the demand dictated by the power grid (Kehlhofer et al., 1999). In order to fulfill these specifications relevant process variables are measured and controlled by control systems, to ensure safe and stable operation of the process including transient load changes, e.g. start-up and shut-downs (Kehlhofer et al., 1999; Montanes, 2018). Excessive drifting of some process parameters from the target set point is prevented by tight regulatory control (Montanes, 2018). One type of control applied on power units is closed loop control. In this case a controller receives measured data from a measuring device, which signal is subsequently forwarded to a control device (usually a control valve) in order to reach the set point of a given process variable (Kehlhofer et al., 1999). The closed control loops used in this investigation can be classified into two groups:

- the main plant load control loop, which includes the conservation of mass throughout the process and the load regulation;
- the secondary control loops, which maintain important process parameters within certain process limits. This might be a pressure, a temperature, a level, etc.

According to Kehlhofer et al. (1999), this distinction is made in the control structure design for combined cycles.

The main objective of process control is to maintain the process at the desired operating conditions (Seborg et al., 2008). For this purpose a top-down analysis is rendered in this work with the overall control objective to operate the power cycle as efficiently as possible at varying steady-state conditions (i.e. loads). This is important for the overall plant economy in order to attain a low cost of electricity by saving fuel costs. Indeed, the amount of heat (fuel) input needed is directly implicated with the plant efficiency. Moving from the upper to the lower layer, the control system design is determined by the maximum number of process variables which can be independently controlled, that is, to define the steady-state control degrees of freedom (N_{FC} or DOF) (Seborg et al., 2008):

$$N_{FC} = N_V - N_E - N_D \tag{1}$$

N_V is the number of process variables, out of which N_E are the independent equations between the process variables and N_D are the disturbance variables. All non self-regulating variables have to be controlled in order to maintain the controlled process stable. The active constraints set in the process simulation are a priori controlled variables, whereas all remaining control degrees of freedom must be allocated among the remaining process variables (Zotică et al., 2019). Moreover, basic variable definitions are provided in Table 1.

The procedure of plantwide control structure design is aimed at meeting following consequent steps (Skogestad, 2004):

(i) Definition of the manipulated variables;

[3] Based on Darde et al. (2009) with adjustment of the values for this specific study.

Table 3
Manipulated and controlled variables of main plant load control loop and secondary control loop for control strategy S1.

Pos.	Manipulated variable	Controlled variable
V1	MV1: Fuel input	CV1: Power
V2	MV2: Oxygen input	CV2: (Constant) Air-to-fuel ratio
V3	MV3: Excess water valve	CV3: Water mass flow rate
V4	MV4: Superheater attemperator	CV4: HPT live steam temperature
V5	MV5: Deaerator extraction line	CV5: Feedwater temperature
V6	MV6: LPT valve	CV6: LPT inlet pressure
V7	MV7: Cooling water input	CV7: (Constant) Condenser pressure
V8	MV8: LPT bypass	CV8: LPT turbine mass flow rate
V9	MV9: ECO1 bypass	CV9: Recycled exhaust gas temperature
V10	MV10: HPT valve	CV10: HPT live steam pressure
V11	MV11: HPT bypass	CV11: HPT mass flow rate
V12	MV12: LPST valve	CV12: Live steam pressure
V13	MV13: LPST bypass	CV13: LPST mass flow rate
V14	MV14: Cooling water input	CV14: (Constant) Cooling mass flow rate
V15	MV15: Cooling water input	CV15: (Constant) Cooling mass flow rate
V16	MV16: Feedwater bypass	CV16: LPT upstream temperature

(ii) Definition of the controlled variables;
(iii) Definition of the control configuration.

Control configuration is defined as the arragement of interconnections between the controlled, measured and maipulated variables (Skogestad, 2004). For this purpose, 16 manipulated and controlled variables are selected (see list of the controlled and manipulated variables, illustrated in Table 3), before the control configuration is defined. Three part-load control strategies are adopted and summarized in Table 2. Changes are affecting two key parameters, the TIT (combustion temperature change) and the pressure in the HRSG or a combination of both. The three control strategies could be seen as a qualitative control method, meanwhile load regulation *via* change in fuel mass flow rate, as a quantitative control method. Indeed, all proposed control methodologies could be seen as quantitative and qualitative control method since loads are changed by activation of the fuel input valve. However, other control strategies and combined methodologies have been run by the simulation tool, but without fulfilling the inflicted function of $\left(\frac{\dot{W}}{\dot{W}_0} \subset (0.6, 1.0)\right)$. Control strategy S1 and S3 have been reduced down to 40% part loads, S2 down to 55%, accordingly.

Some assumptions and boundary conditions are listed as follows:

(i) The assumption for the off-design simulation is to be in steady-state condition;
(ii) The maximum turbine inlet temperature (i.e. TIT) of the high temperature turbine is set to be $T_{max} = 1400\ ^{\circ}C$ and is limited by the strength of materials and the cooling system of the >gas turbine (Nord and Bolland, 2020). It is to be noted, that advanced-class gas turbines reach maximum gas turbine inlet temperatures of 1500 $^{\circ}C$, enabling thereby higher efficiencies according to the Carnot priniciple (which defines mean effective heat addition and rejection temperatures Gülen, 2019);

Table 4
Part-load performance of the Graz Cycle with CO_2 capture for control strategy S3.

Net overall load [%]	Sanz et al. (2005)	This study						
	100	100	90	80	70	60	50	40
Thermal cycle efficiency [%]	66.5	66.3	65.8	64.9	63.7	62.2	60.2	57.7
Net electrical cycle efficiency (incl. losses) [%]	64.6	64.4	63.9	63.1	62.0	60.5	58.5	56.0
Efficiency considering O_2-supply [%]	54.8	55.1	54.6	53.8	52.6	51.1	49.2	46.7
Net efficiency (incl. CO_2-compression) [%]	52.6	53.1	52.6	51.8	50.6	49.1	47.2	44.7
HTT power [MW]	120.27	95.49	86.94	78.76	70.77	62.90	55.04	47.13
Relative HTT load [%]	100.0	100.0	91.0	82.7	74.1	65.9	57.6	49.4
Total turbine power [MW]	142.75	113.53	103.13	93.21	83.58	74.12	64.70	55.26
Total compression power [MW]	47.16	37.12	34.35	32.07	30.06	28.22	26.43	24.61
Electrical power output (incl. losses) [MW]	95.59	73.73	66.36	58.99	51.61	44.25	36.87	29.49
O_2generation and compression [MW]	14.15	10.64	9.67	8.72	7.78	6.85	5.91	4.98
CO_2compression to 100 bar [MW]	3.12	2.19	1.99	1.80	1.62	1.41	1.34	1.25
Net power output [MW]	78.32	60.90	54.70	48.47	42.21	35.94	29.62	23.26
Total heat input [MW]	143.44	113.75	103.38	93.22	83.20	73.24	63.28	53.27
CO_2-purity at the exhaust gas drain [%]	92.0	90.5	90.4	90.3	90.2	89.9	89.1	87.4
Working fluid composition after HTT [mol%]								
H_2O	77.1	75.8	75.8	75.9	76.0	76.2	76.5	77.0
CO_2	22.2	22.0	22.0	21.9	21.8	21.6	21.3	21.0
N_2	0.2	0.6	0.6	0.6	0.6	0.6	0.6	0.6
O_2	0.4	0.4	0.4	0.4	0.4	0.4	0.4	0.4
Ar	0	1.1	1.1	1.1	1.1	1.1	1.1	1.1
HTT inlet temperature [°C]	1400.0	1400.0	1400.0	1400.0	1400.0	1400.0	1400.0	1400.0
HTT exhaust gas temperature [°C]	579.4	568.7	566.9	563.6	558.8	552.4	544.0	532.8
HTT inlet pressure [bar]	40.0	40.0	36.4	32.9	29.6	26.2	22.9	19.5
HTT outlet pressure [bar]	1.053	1.053	0.964	0.879	0.795	0.714	0.632	0.550
HPT inlet temperature [°C]	549	554.1	547.0	538.8	529.3	517.8	503.7	485.6
HPT inlet pressure [bar]	180.1	185.1	167.7	151.4	135.8	120.6	105.5	90.5
LPT inlet temperature [°C]	216.1	203.2	204.5	205.7	207.1	208.6	210.8	213.9
LPT outlet pressure [bar]	0.041	0.041	0.041	0.041	0.041	0.041	0.041	0.041
C1/C2 pressure ratio [-]	41.2	41.2	41.1	41.0	40.8	40.7	40.4	40.1
C1 inlet temperature [°C]	96.7	102.2	100.7	98.3	95.3	91.5	86.9	81.2
Minimum temperature difference in the HRSG [°C]	5.0	5.0	4.4	3.9	3.4	2.9	2.4	2.0
Cooling steam mass flow ratio [%]	13.7	13.4	13.9	14.7	15.9	17.3	19.3	22.0
Recycled stream mass flow ratio [%]	55.1	53.7	53.9	54.3	54.7	55.2	55.8	56.6
Relevant mass flows rates [kg/s]								
Fuel mass flow	2.89	2.45	2.22	2.01	1.79	1.58	1.36	1.15
O_2 mass flow	11.55	10.07	9.15	8.25	7.36	6.48	5.60	4.71
CO_2 mass flow to storage	8.91	7.30	6.64	6.00	5.40	4.87	4.45	4.16
C1/C2 mass flow	45.29	34.72	31.90	29.26	26.71	24.21	21.72	19.22

(iii) A well-tuned air-to-fuel-ratio controller is assumed. A constant oxygen excess of 3% is assumed, i.e. $\lambda^{sp} = 1.03$;
(iv) Upper temperature limit for the HPT is equal $T_{\max} = 600\ ^{\circ}C$;
(v) Partial-arc admission turbines are not represented as a viable control strategy in this study. A partial admission turbine is less efficient than a standard turbine due to following reasons (Zaryab et al., 2020):
- The first turbine stage must feature a near-zero reaction degree in order to avoid fluid dynamic losses;
- A portion of the rotor's mechanical power to fluid is lost due to "windage losses";
- Mixing losses in the surrounding area of the jet and the stagnant fluid.

(vi) No compressor maps considering VIGVs are implemented in this study. For simplicity reasons an alternative approach is to be selected similar to the one done by Sanz et al. (2018);
(vii) The HRSG is assumed to be a once-through type. Low pressure in the boiler is possible, but results in higher capital costs of the heat exchange equipment. Pressures are constrained between 0.5 and 1.053 bar. Heat losses in the HRSG are neglected;
(viii) No modelling and simulation of the ASU has been performed. The assumption made is, that the ASU maintains the same specific energy consumption at partial load conditions as at full load. The same is valid for the CO_2 CPU at the exhaust gas drain. The values used are described in Section 2.1. For further details it is referred to Darde et al. (2009) and Lockwood (2014);
(ix) For the cooling system of Graz Cycle a direct water cooling of the condenser is chosen. For this purpose, the power plant needs to be located near a river, a ocean or a cooling pond (Nord and Bolland, 2020). This type of cooling enables the lowest possible condenser pressure, i.e. 0.041 bar. One option to operate the condenser in part-load is to keep the cooling water mass flow rate constant, regardless the decreased load. By doing that the cooling water pumps are operated at constant speed. In this study, the condensate pumps are operated to keep the condenser pressure constant. The condenser is supplied with cooling water at an average temperature of 10 °C. Note, that the condenser after the LPT is the only model of the part-load simulation which is kept for simplification in steady-state mode. The product of heat transfer coefficient times area ($k{\cdot}A$) is not set as an active contraint. For more information see Section 2.3.
(x) Hotwell levels are not controlled and neglected in the process scheme. The deaerator is modelled like a simple heat exchanger;
(xi) There are two feedwater pumps present in the Graz Cycle scheme. Due to its negligible power demand in relation to the compressors, any performance map or part-load operation model for pumps is implemented and isentropic pump efficiencies are kept constant at partial loads. The pumps are not actively controlled but run on constant rotational speed as it must always provide the same pressure head of 1 bar and 213 bar, respectively. Thus, both downstreams are controlled variables.

2.3. Modelling

A thermodynamic-based model of a 60 MW Graz Cycle is used to study optimal performances and control operation. For this purpose, the simulation tool IPSEpro was utilized to built the steady-state models and to perform the process simulation (SimTech Simulation Technology, 2017). The following paragraphs describe the modelling of the power plant components, i.e. simplified equations to describe the operation of the main equipment.

Steam turbine

The first law of thermodynamics or conservation law of energy states that energy in an isolated system can neither be destroyed nor produced, but only be converted. The total energy in a closed system remains constant and the only way to change it is through energy transferred across the system boundaries in form of work or heat. Thus, the steam turbine power generation $\dot{W}_{ST}$ can be expressed as follows (Boyce, 2002):

$$\dot{W}_{ST} = \dot{m}_s \eta_m \eta_s \left(h_{feed} - h_{s,drain}\right), \tag{2}$$

where $\dot{m}_s$ is the feed steam mass flow rate, η_m the mechanical efficiency, η_s the isentropic efficiency and $(h_{feed} - h_{s,drain})$ the isentropic enthalpy drop between inlet and outlet section. The enthalpy term can be further reduced by $dh = c_p dT$. In order to approximate the characterstic curve (i.e. turbine map) of the steam turbine, which describes its part-load performance, Eq. (3) is applied for modelling. Referring to the so-called Stodala law (Stodala, 1910), the changes of the mass flow, inlet and outlet pressures and inlet temperature of the steam in part-load (in comparison to nominal load) conditions follows this relation:

$$\frac{\dot{m}_s}{\dot{m}_{s,0}} = \frac{\sqrt{\frac{p_a^2 - p_\omega^2}{T_f}}}{\left(\sqrt{\frac{p_a^2 - p_\omega^2}{T_f}}\right)_0}. \tag{3}$$

The efficiency of the steam turbine depends on the enthalpy drop. At off-design conditions there is not a great alteration in the enthalpy drop except in the last turbine stages. Therefore the polytropic efficiency in the superheated area can be set constant (Kehlhofer et al., 1999). The isentropic efficiency η_s of the steam turbine (i.e. the comparison between the real and ideal expansion in a turbine) is a correlation of the mass flow rate (Jüdes et al., 2009):

$$\frac{\eta_s}{\eta_{s,0}} = -1.0176\left(\frac{\dot{m}}{\dot{m}_0}\right)^4 + 2.4443\left(\frac{\dot{m}}{\dot{m}_0}\right)^3 - 2.1812\left(\frac{\dot{m}}{\dot{m}_0}\right)^2 + 1.0535\left(\frac{\dot{m}}{\dot{m}_0}\right) + 0.701. \tag{4}$$

At part-load operation, the efficiency η_s has to be adjusted according to changes in the exit steam quality Δx_e. If the outlet steam quality x_e is lower than 1, following approximation is valid (Jüdes et al., 2009):

$$\eta_{s,corr} = \eta_s - \frac{1}{2}\Delta x_e, \tag{5}$$

where $\eta_{s,corr}$ denotes the corrected value of the isentropic efficiency by taking into account the steam quality. According to Fig. 3, all blue coloured turbines are modelled by means of the Stodala equation, i.e. LPT turbine, LPST turbine and HPT turbine.

Cooled gas turbine Again, the first law of thermodynamics is applied for sake of the power production of the gas turbine asset. The gas turbine power performance is calculated by means of Eq. (6) Boyce (2002).

$$\dot{W}_{GT} = \dot{m}\, \eta_m \eta_s \left(h_3 - h_{s,4}\right), \tag{6}$$

where $\dot{m}$ is the hot gas mass flow rate, η_m and η_s the mechanical and isentropic efficiency, and $(h_3 - h_{s,4})$ the enthalpy drop to the isentropic line.

To approximate the off-design operating map of a gas turbine (i.e. HTT) the chocked nozzle equation is used. Chocked flow means that the mass flow does not increase even if there is a further decrease in the downstream pressure. The chocked nozzle equation relates mass flow rate, inlet temperature and inlet pressure at the actual point of operation to the nominal (i.e. design) point of turbine operation (Ulfsnes et al., 2003). It is inversely proportional to the square root of the molecular weight, which has to be taken into account if the working fluid molecular weight changes during the process through steam injection in the turbine. More precisely, the chocked nozzle equation states:

$$\left(\frac{\dot{m}\sqrt{T}}{p\sqrt{MW}}\right)_3 = \left(\frac{\dot{m}\sqrt{T}}{p\sqrt{MW}}\right)_{3,0}. \tag{7}$$

The molecular weight (MW) is not being neglected in the process modelling. However, the isentropic efficiency can be assumed constant at part-load operation as a valid assumption of a gas turbine performance map ($\eta_s = \eta_{s,0}$) (Ulfsnes et al., 2003; Zaryab et al., 2020).

Although the part-load equation for the gas turbine is relatively simple, the cooled gas turbine model used here is all the more complex. It was developed at the Institute of Thermal Turbomachinery and Machine Dynamics (Graz University of Technology) and is built on a stage-by-stage methodology similar to the work presented by Jordal et al. (2003). The model calculates the necessary cooling mass flow rate per stage. It assumes that half of the cooling mass is injected to the stage at the inlet and the rest at the outlet. The mass flow rate of the cooling medium is calculated by:

$$\dot{m}_c = \dot{m}_1 \frac{(h_3 - h_{4a})\left(\frac{T_3+T_{4a}}{2} - T_{metal}\right)}{\vartheta\left(h_{k\left(T_{metal}-\Delta T_{cooling}\right)} - h_{k(T_k)}\right)}. \tag{8}$$

The turbine blade surface has a prescribed maximum metallic temperature (T_{metal}), which is not allowed to be exceeded. A minimum temperature difference of 150 °C between the surface temperature of the blade and the cooling medium at the outlet of the blade holes is assumed. The denominator's expressions are: $h_{k(T_{metal}-\Delta T_{cooling})}$ is the specific enthalpy of the cooling medium at the outlet of the cooling holes, $h_{k(T_k)}$ is the specific enthalpy of the cooling medium at the inlet and ϑ is the thermal resistance of the blades, explained by Eq. (9).

$$\vartheta = \frac{T_3 - T_{4a}}{f_A\, n_{st}\, St\, \frac{1}{sin(\beta_2)}}, \tag{9}$$

where f_A is the ratio of blade surface area to axial passage area, n_{st} the number of turbine stages and β_2 the relative angle of the velocity triangle at the rotor outlet. The cooling steam, once it left the turbine blade, also expands with the main flow and produces additional power.

Compressor Most gas turbine applications use axial-flow compressors. In order that the fluid enters the first stage of rotors at the desired flow angle, an additional row of variable blades, called variable inlet guide vanes (VIGVs), are introduced (Boyce, 2011).

The expression for calculating compression work is following (Boyce, 2002):

$$\dot{W}_C = \dot{m}\,\eta_m \eta_s \left(h_{s,2} - h_1\right). \tag{10}$$

In a compressor operating diagram, the lines of constant reduced speed are vertical. For constant speed, i.e. constant velocity v in the equation of continuity, constant volumetric swallowing capacity can be assumed, and thus following is stated (Nord and Bolland, 2020):

$$\left(\frac{\dot{m}RT}{pA_c}\right)_1 = \left(\frac{\dot{m}RT}{pA_c}\right)_{1,0}. \tag{11}$$

The cross-sectional inlet area of the compressor can be considered constant, unless VIGVs are used to control the flow rate (Nord and Bolland, 2020). Here, the compressors are modelled using Eq. (11). For the simulation a very simple approach was used. Instead of considering a compressor map, the efficiency was varied according a cubic spline through following three points:

$$\left(\frac{\eta}{\eta_{s,0}}\right)^1_+ := \left\{ \begin{array}{lll} 0.5 & for & \frac{m_f}{m_{f,0}} = 0.1 \\ 1 & for & \frac{m_f}{m_{f,0}} = 1.0 \\ 0.8 & for & \frac{m_f}{m_{f,0}} = 1.5 \end{array} \right\}. \tag{12}$$

Heat exchanger and condenser The description of the steady-state off-design performance of the heat exchangers requires additional equations. Indeed, the equation for heat balance is primarily set by the transferred heat, i.e. $\dot{Q} = k{\cdot}A{\cdot}\Delta T_{\log}$. The logarithmic mean temperature difference (i.e. $\Delta T_{\log}$) is represented in Eq. (13) Kehlhofer et al. (2009).

$$\Delta T_{\log} = \frac{\Delta T_A - \Delta T_B}{ln\left(\frac{\Delta T_A}{\Delta T_B}\right)}, \tag{13}$$

where subscript A stands for the temperature difference of the two streams at one end side and B for the other side. Since the heat exchanger surfaces are fixed, the conditions on the water/steam side and on the flue gas side within the heat exchanger change, and so does the overall heat transfer coefficient (Nord, 2010). Thus, Eq. (14) states:

$$\frac{k{\cdot}A}{(k{\cdot}A)_0} = \left(\frac{\dot{m}_h}{\dot{m}_{h,0}}\right)^m. \tag{14}$$

The exponent m is component specific and depends on the geometry of the heat exchanger (Jüdes et al., 2009). Its value is assumed to be 0.58 (i.e. for staggered tubes) (Nord, 2010). Moreover, the pressure drop decreases in the heat exchanger during part-load operation and is defined as follows (Nord, 2010):

$$\frac{\Delta p}{\Delta p_0} = \left(\frac{\dot{m}}{\dot{m}_0}\right)^2. \tag{15}$$

In this study, all heat exchangers and condensers are modelled by assuming a counter-flow configuration.

3. Plantwide control strategies

This chapter describes the main plant load control loop and the secondary control loop for the Graz Cycle. Compared to combined cycles, oxy-combustion cycles do not have clear-cut separation between topping high temperature Brayton cycle and bottoming low temperature Rankine cycle as they are usually integrated and contain energy and mass recycle. Nevertheless, the differentiation between the two main control loops is essential. Controls and automations build a relatively complex system and thus control structures have to be applied logically in order to result in a hierarchic distributed architecture (Boyce, 2002; Kehlhofer et al., 1999). More precisely, in this work it is assumed that the main plant load control loop coordinates the operation of the entire power plant, whereas the secondary control loops fulfill functions on a subordinated layer.

3.1. Main plant load control

In Fig. 3 the principle Graz Cycle (GC) main plant load control structure is illustrated. Depending on the demand of the electrical grid an operating point P^{sp} (i.e. power set point) is determined by the overall load controller. This control unit is on the top of the control system, and supervises control variables, which are significant on an overall point of view, i.e. the supervisory control layer (Zotică et al., 2019). Furthermore, this layer is in charge of load changes (i.e. load/frequency control) (Montanes, 2018). More precisely, the overall load controller receives values from the lower layers, in this case the load points from the two generators, and communicates downwards (i.e. from the upper to the lower layers) by sending eventual adjustments to the combustion controller. From the feedbacks in turn, it determines whether it is necessary to make any load corrections. In practice, the application of a combined load/frequency controller has proved its worth (i.e. $\dot{W}$ for electrical power output, and ω_T for turbine frequency) (Kehlhofer et al., 1999; Lechner and Seume, 2018). Nevertheless, the remarks are valid for both. The question, which variable sets the target, boils down to whether the generator runs under synchronous condition on the electrical grid or not (e.g. manual load control from the operator of a peak load power plant to load target point) (Lechner and Seume, 2018).

Moving downwards, the combustion controller tunes the set point of the fuel mass flow rate (i.e. $\dot{m}^{sp}_{fuel}$) of the flow controller and the control

mechanism of opening/closing of the variable inlet guide vanes (VIGVs) (Kehlhofer et al., 1999; Mehrpanahi and Payganeh, 2017). It receives an actual measured value of the turbine exhaust gas temperature (TET) by means of a temperature transmitter. Since it is not possible to directly measure the turbine inlet temperature (known as TIT), values of the turbine pressure ratio and the turbine exhaust gas temperature are used to calculate an "inferred" TIT (Gülen, 2019; Kehlhofer et al., 1999; Moon and Kim, 2020). To sum up, three routes exist to vary the gas turbine's power output *via* combustion controller (Gülen, 2019):

(i) Compressor inlet mass flow rate change (i.e. by opening or closing of VIGVs);
(ii) Firing temperature change (i.e. by increasing or reducing fuel flow rate);
(iii) A combination of both.

The fuel (heat) input consequently determines the oxygen demand of the combustor, which is controlled by the air-to-fuel ratio controller, which regulates the oxygen valve V2, such that a constant O_2 excess ratio is maintained. The fuel (NG) and O_2 streams enter the combustor separately. It is assumed that both of these streams are measured and that the ratio controller fixes the oxygen inlet valve opening (Imsland et al., 2004; Sinnott, 2005). Accordingly, whenever a load change takes place, the fuel mass flow is changed and thereby the oxygen inlet mass flow. Note, that all controls and feedbacks discussed so far directly depend on the setting of the overall load controller.

On the other hand, the water valve controller (i.e. WVC) is self-dependent and works by means of the logic explained in Fig. 3. Three measured variables are taken as inputs, i.e. $\dot{m}_1$, $\dot{m}_2$ and $\dot{m}_3$. The amount of water generated in the combustion chamber is calculated through the reaction equation, molar masses and the fuel mass flow rate ($\dot{m}_1$), i.e. an output signal of the flow measurement of the natural gas source. The trend of the water mass flow rate in the exhaust gas drain under different load conditions is illustrated in Fig. 5. It is derived by the flow measurement at the gas drain ($\dot{m}_2$) and the corresponing simulation-based H_2O mass content. The pure water mass flow rate ($\dot{m}_3$) stems from the water separator after the cooler before the CO_2 compression and purification unit (CPU). The continuity equation (i.e. conservation of mass) for the process water is following at steady-state:

$$\frac{dm_{H_2O}}{dt} = \sum \dot{m}_{in} - \sum \dot{m}_{out} = 0 \tag{16}$$

The limit for the mass flow rate of valve V3, i.e. $F_{\min} \geq 0$, defines the valve as a sink. Indeed, the water drain does not act as a source.

As stated before, oxy-combustion cycles are distinguished substantially from conventional combined cycles by the recycled mass and energy rate. For this reason, the recycled mass ratio has to be fixed somehow. More precisely, in this investigation, it is set on one end by the sucking capacity of the compressors C1 and C2, which rotate on the same shaft with fixed rotational speed, and on the other end by the back-pressure of the low pressure turbine throttle (i.e. a valve). For the precise turbomachinery arrangement it is referred to Sanz et al. (2004).

Concerning the compressors, the most common approach to achieve optimal part-load performance is the use of VIGVs, placed upstream of the first compressor stage, in order to generate arbitrary power (Mehrpanahi and Payganeh, 2017; Zaryab et al., 2020). Thus, the mass flow rate through the compressor is reduced by rotating vanes (i.e. the VIGVs are closed) (Gülen, 2019; Snarheim et al., 2005; Zaryab et al., 2020). As such, VIGVs adjust the effective flow area and hereby the volumetric flow capacity of the compressor (which otherwise is constant for constant rotational speed) (Gülen, 2019). It is to be noted, that VIGVs are fully open for generating nominal power (i.e. at full load operation) (Mehrpanahi and Payganeh, 2017). By closing the VIGVs, the gas turbine forfeits in efficiency, but the heat flow to the HRSG is increased, which leads to a gain in the combined cycle efficiency (Snarheim et al., 2005).

Once a power plant is installed and commissioned, it operates across a wide range of different load operating conditions (Gülen, 2019). Here, by taking into account the interconnection between power plant and grid, a possible load change could be:

- The frequency of the electrical grid may vary by 1%. An important aspect of the load/frequency control are rapid fluctuations in the electricity grid (Kehlhofer et al., 1999). The adaptment to this variations are known as frequency response and have to happen normally within seconds (defined by grid codes). The droop setting (i.e. a proportional controller which distributes the load between the electrical generators connected in parallel (Zotică et al., 2019)) might be 5%, which means that a frequency drop of 5% is counteracted by a load increase of 100%. In this context, a frequency drop of 1% causes a gas turbine (i.e. the HTT turbine) load jump of 20%, and a steam turbine load change of 0%, because the droop characteristic for the steam turbine is only valid for rising frequencies (Kehlhofer et al., 1999). Since the HTT is accounting for approximately 85% of the overall power, i.e. a change of power of 20% in the gas turbine load gives 20%·0.85 = 17% overall load increase of the power plant. This is determined by the overall load controller. For instance, for an actual net overall load of 73%, plus 17% of load increase results in 90%. According to this load target set point, the overall load controller forwards the set point for the turbine inlet temperature (TIT) to the combustion controller.
- The temperature set point for the high temperature turbine TIT might be 1400 °C.[4] Accordingly, the combustion controller determines the fuel mass flow rate by sending a set point to the flow controller at the natural gas inlet (i.e. a fuel mass flow rate equal to 2.22 kg/s at 90% load) and the VIGVs setting of the compressor C1 pursuant the desired load point. Note, that for constant turbine inlet temperature (or firing temperature) the compressor inlet flow rate *via* VIGVs sets the load (Gülen, 2019). Excessive drifting of process parameters are counteracted by fast gas turbine regulatory control to achieve steady-state conditions.
- Promptly the ratio controller FFC sets the oxygen mass flow rate and manipulates the valve V2 (i.e. a throughput manipulator) by means of the air-to-fuel ratio λ and the measured fuel mass flow. In practice, for $\lambda^{sp} = 1.03$ and appointed natural gas inlet flow at 90% load, the oxygen mass amounts to 9.15 kg/s.
- The water valve controller input consists of three mass flow rates, i.e. the combustion generated water (depending on $\dot{m}_1$), the water content in the exhaust carbon dioxide drain (depending on $\dot{m}_2$) and the pure excess water from the separator ($\dot{m}_3$). To sum up, the WVC defines the amount of water to be extracted for valve V3. In this case the exhaust gas drain composition represents the disturbance. However, the controller is able to react quickly depending on mass flows across the system boundaries and not depending on certain load target set points from the overall load controller. At 90% load, 4.15 kg/s of water is extracted from valve V3.
- The VIGV angle of compressor C3 is set by means of the frequency ω_C. It is noteworthy, that at part loads the inlet guide vanes are partially closed (i.e. at full-load operation VIGVs are hence completely open) (Mehrpanahi and Payganeh, 2017).

3.2. Secondary plant control

The secondary control loops P&ID for one of the control strategies (S1) discussed in the paper are illustrated in Fig. 4. In this subsection, controlled and manipulated variables of the Graz Cycle shall be briefly explained (see Table 3), before the different control strategies are discussed. Note, that the listing in Table 3 is provided for control strategy

[4] This value - so as the following - is exemplary for control strategy S3 and is mapped in Table 4.

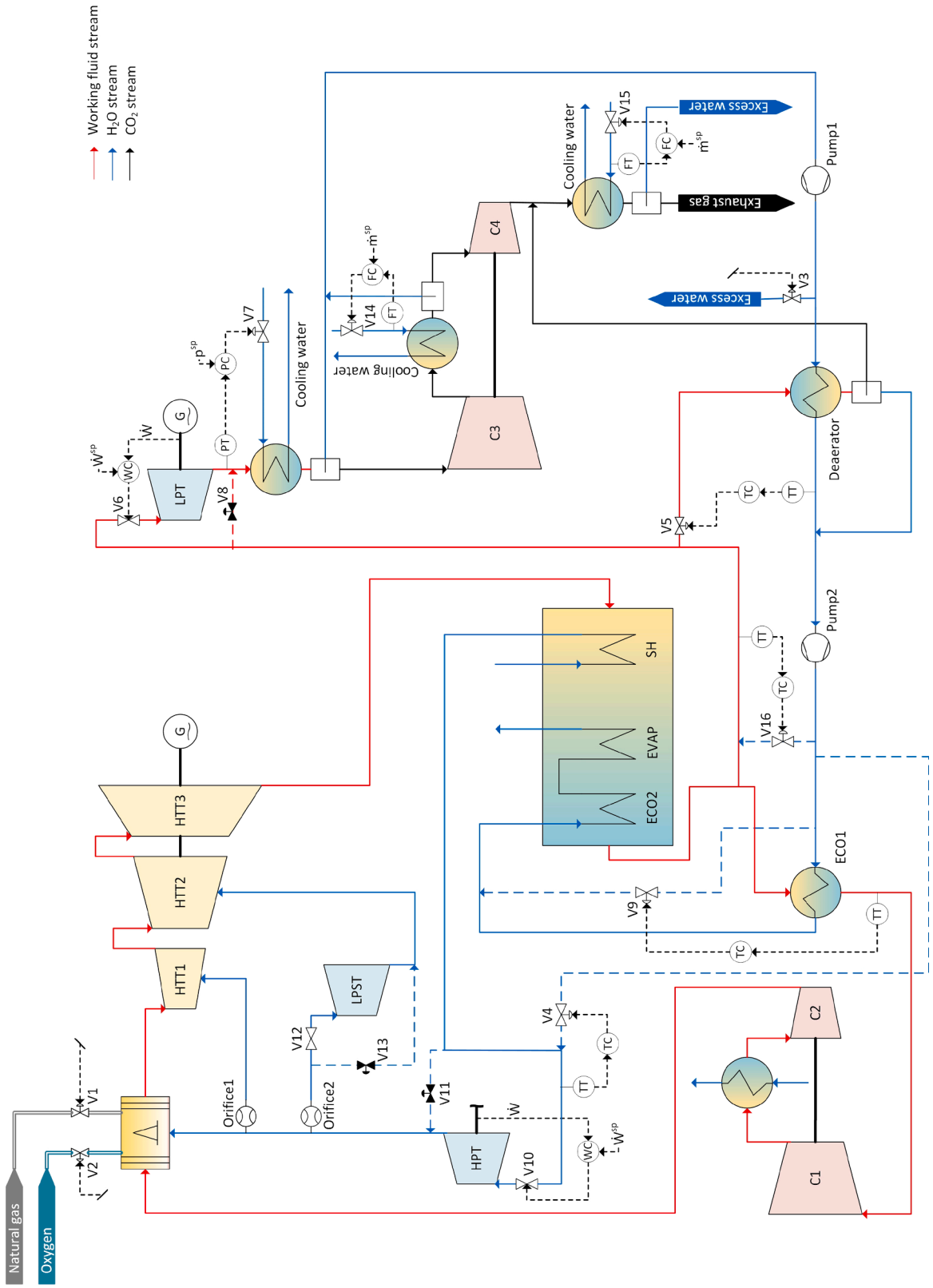

Fig. 4. Secondary control loops for the control strategy S1 of the Graz Cycle.

S1 as instance. The first three variables are part of the main plant load control loop and are already discussed in the previous section. Generally, the selection of controlled variables occured in a way, that the optimal operation is maintained despite possible disturbances, which may occur (Zotică et al., 2019).

By adding a part-load model to the steady-state model, a control degree of freedom is lost. That way, "pairings" for the active constraints are formed. For example, valve V3 is characterised as manipulated variable MV3, which controls the circulating water mass flow rate (i.e. controlled variable CV3) within the process by activation of the excess

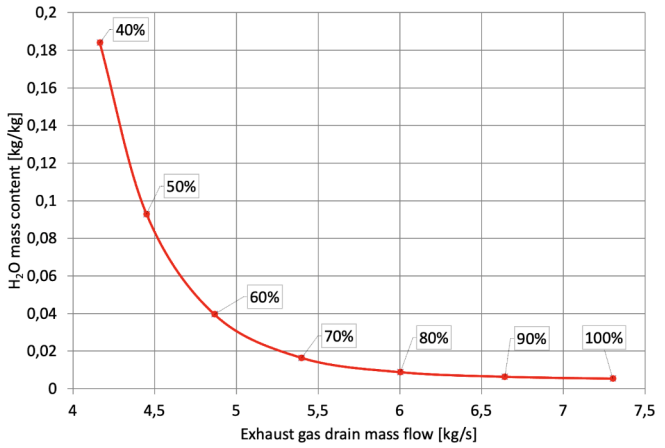

Fig. 5. The control curve for the water valve controller. The plot indicates the water mass content of the exhaust gas drain, i.e. $\dot{m}_2$, at different load points (e.g. for control strategy S3).

water valve (i.e. MV3). Here, the pair-close rule is applied and "pairings" are listed accordingly in Table 3 (Zotică et al., 2020). For instance, on the regulatory layer the resulting "pairings" are:

- Application of fuel input (MV1) to control the power (CV1);
- Application of oxygen input (MV2) to the constant air-to-fuel ratio (CV2).

The control of the condenser pressure is done by regulation of valve V7, which adjusts the cooling water mass flow. The cooling water keeps the condenser pressure constant. Instead, the control of the condenser could have also been designed in such a way, that the cooling mass flow rate is kept constant (such control is common in practice), which is applied for the coolers following compressor C3 and C4, respectively. Here, the correlation is following: control of cooling water through regulation of valve V14 (or V15) and thereby attaining constant cooling mass flow rate. In this case, constant cooling mass flow leads to a decrease in condenser pressure due to a decrease in ΔT for the cooling flow at part loads.

Due to the fact that start-ups and shutdowns are not considered in this work, the bypasses (for example valve V8 for the LPT bypass) are normally closed and mass flows are equal to zero. Bypasses are necessary, when the energy in the feed becomes larger than the power demand, to avoid very high pressure levels (Zotică et al., 2020).

For precise control of the live steam temperature of the HPT, an attemperator is installed after the superheater. High pressure liquid water is sprayed into the live steam in order to cool it down to the required temperature (Kehlhofer et al., 1999). Usually, if the heat recovery steam generator is of the once-through sort, the live steam temperature is regulated by the feed water flow out of the feed pumps, however, at extreme load conditions and during start-ups, attemper is still needed (Kehlhofer et al., 1999). The HPT turbine uses throttle control. Indeed, the live steam pressure at the inlet section of the HPT is controlled with the steam valve, to wit the power produced (measured variable) is controlled by adjustments of the valve V10 (i.e. a thoughput manipulator). This arrangement is a standard industrial control structure, so-called turbine driven operation (Zotică et al., 2019). The turbine driven operation strategy has the advantage that the response time to load changes is fast. However, having the valve only partly opened, it results in throttling losses at the turbine inlet (Zotică et al., 2019). Throttling intrinsically means a reduction in pressure without energy loss in form of heat and/or work. Therefore, by applying the first law of thermodynamics to the system an isenthalpic process is obtained. The second law of thermodynamics leads to the irreversibility of the process, furthermore to an obvious increase of entropy and related exergy losses by decreasing the available turbine work (Zotică et al., 2020).

The LPST operates in floating pressure operation, i.e. the valve V12 is kept fully open in order to minimize throttling losses and therefore the live steam pressure is left uncontrolled. This operation mode is optimal from an energy point of view, but, due to the inertia of the boiler, it has a slow time response for load changes (Zotică et al., 2019).

For the control loop shown in Fig. 4 deaerator heating is done by working fluid extraction at the LPT feed. The manipulated variable MV5 controls the deaerator extraction line by measuring the temperature of the water stream at the deaerator outlet. According to the Carnot theorem the temperature of the feedwater at the condenser exit should be as low as possible in order to allow optimum utilisation of the heat available. Indeed, this is one of the Rankine cycle characteristics, which the Graz Cycle follows. However, the feed water pre-heating is primarily done to avoid low temperature corrosion; its temperature must not, even at lower loads, drop significantly below the water dew point (Kehlhofer et al., 1999).

Pumps and orifices are not actively controlled during operation. The first pump after the condenser (i.e. Pump1) boosts low pressure water to the deaerator pressure (i.e. $p^{sp} = 1$ bar), the second (i.e. Pump2) increases the pressure level even more ($p^{sp} = 213$ bar) and feeds water to the economiser. Both pumps are running at constant speed (i.e. a constant pressure gradient).

The investigation about the control and automation of the Graz Cycle led to three different strategies, presented in Table 2. The three strategies bring forth different results and efficiencies in the part-load simulation and are analysed in Chapter 4. They differ from each other in the secondary control loop, which maintains the important process parameters such as flow rates, temperatures, pressures, and compositions at all operating conditions. Indeed, the usage of variable guide vanes for the compressors C1/C2 and C3/C4, respectively, is coupled with a speed control system of compressor shafts in order to regulate their mass flow. The application of VGVs, which allows optimal part-load and start-up performances, is discussed in the next chapter. First, the three control strategies are presented.

For control strategy S1 the following considerations are valid. As it is shown in Table 2, the key controlled variables are the power output, the HTT downstream pressure (i.e. 1.053 bar) and the condenser pressure (i.e. 0.041 bar). The set point for produced power (characterised as $\dot{W}$) is set by means of the main plant load control loop discussed in Section 3.1. The remaining DOFs should be used to keep the efficiency as high as possible while meeting important process constraints (Snarheim et al., 2005). The control strategy S1 uses two orifices to control the cooling mass flow ratio to the HTT1 and the HTT2, like illustrated in Fig. 4. Indeed, orifices fix the split ratios between the main stream and the turbine cooling water stream. Note, that in control strategy S1 the HTT inlet temperature is not constant, but instead it depends on the respective load point.

If a conventional HRSG is used for the Graz Cycle the outlet temperature of the HTT would normally be kept constant at atmospheric pressure range, due to the wall thickness in the OTSG. However, it is not given beforehand that the steadiness of the pressure in the HRSG is beneficial in terms of efficiency for this process. For the low pressure turbine, a throttle control (i.e. a throughput manipulator) is used.

The control strategy S2 (cf. Fig. 6) uses a throughput manipulator instead of throttle control Orifice1. Indeed, the arrangement of the manipulated variable MV17 is changed, i.e. a valve, which is turbine driven sets the inlet cooling ratio by means of the turbine power output of HTT1. The released degree of freedom allows to keep the TIT constant. The control strategy of maintaining the turbine inlet temperature high as the mass flow is reduced, is commonly used in gas turbines. According to the principle of the Carnot cycle this strategy is paid off in terms of efficiency. Basically, the method of cooling the free-running turbine HTT1 is changed. As for control strategy S1, the LPT turbine is subject to throttle control.

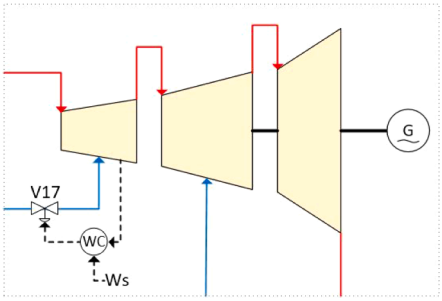

Fig. 6. Section of the closed control loop of control strategy S2 and S3 illustrating the control of the cooling stream to the first section of the turbine (i.e. HTT1).

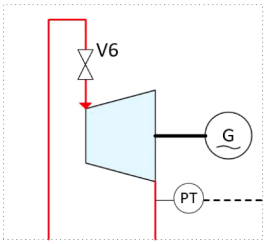

Fig. 7. Section of the closed control loop of control strategy S3 illustrating the turbine (i.e. LPT) in floating pressure operation mode.

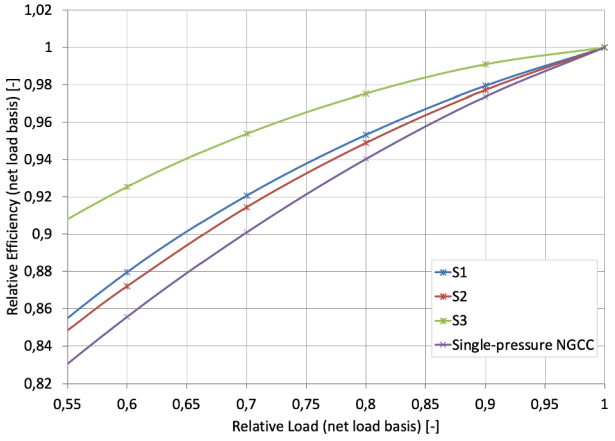

Fig. 8. Optimal steady-state net efficiencies for three different GC control strategies when operating at part loads. The three strategies are compared to a readily available technology, i.e. a single-pressure natural gas combined cycle.

In control strategy S3 the pressure in the HRSG is allowed to vary. As it is shown in Table 2 the outlet pressure of the HTT turbine depends on the power cycle output (i.e. $p(\dot{W})$). The LPT uses floating pressure operation and follows the gas turbine outlet pressure by generating power with whatever steam conditions provided by the OTSG, see Fig. 7. If higher overall plant efficiencies are obtained by the variability of the HRSG pressure is investigated in following chapter. After a high temperature turbine load change, the LPT load follows automatically with a few minutes delay depending on the response time of the heat recovery steam generator (Kehlhofer et al., 1999). The slow response for load changes is the disadvantage of floating pressure operation (Zotică et al., 2019). However, this kind of automation technique is very common in industrial combined cycle plants. As indicated in Table 2, the strategy S3 has no Orifice1, instead it uses a throttle operation mode for the HTT1 cooling stream, as discussed also for strategy S2.

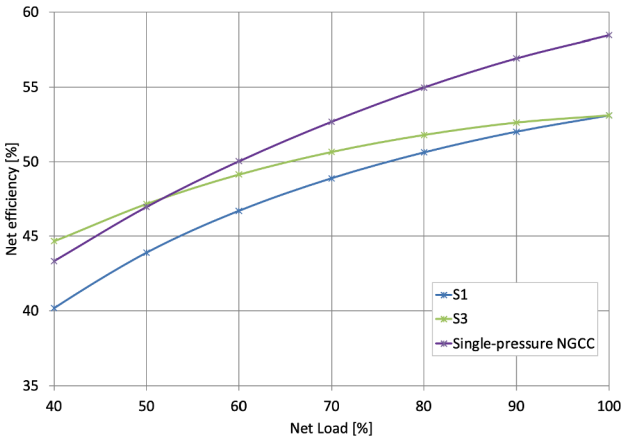

Fig. 9. Comparison of net efficiencies between strategy S1, S3 and a NGCC by reducing loads down to 40%.

4. Results

Since the Graz Cycle is different from common combined cycles and has a recycled mass flow rate, it is not a priori self-evident how the cycle reacts in part-load conditions and how far the cycle load can be reduced. Fig. 8 shows the effect of the control strategies compared in terms of efficiency at part-load operation, where a relative load value means the actual net power value of the power plant (incl. O_2-supply and CO_2-compression) divided by the value when the power cycle is operated at its design point (i.e. $\frac{\dot{W}}{\dot{W}_0}$) (Snarheim et al., 2005). The load is decreased down to 40% of the nominal load. The efficiency is calculated as Eq. (17) states:

$$\eta_{net} = \frac{\dot{W}_{out} - \dot{W}_{O_2} - \dot{W}_{CO_2}}{\dot{m}_{NG} \cdot LHV}, \tag{17}$$

where LHV is the lower heating value of the natural gas feed and $\dot{W}_{out}$ is the total produced power from the turbines minus the power of the compressors and pumps. The value $\dot{W}_{O_2}$ represents the oxygen generation and compression and $\dot{W}_{CO_2}$ is the CO_2 compression to 100 bar.

4.1. Ideal part-load operation

Optimal part-load operation consists in a reduction of the fuel mass flow rate (i.e. $\dot{m}_{NG}$) proportional to the turbine mass flow rate and the net power production just like that the pressures and temperatures of the power cycle remain constant compared to design-point values (Zaryab et al., 2020). Such a way would guarantee that the efficiency remains equal all the time. However, practically this is not possible since operating maps of different cycle components (such as a turbine, a compressor, a pump or a heat exchanger) cause cycle pressure and temperature variations. The efficiency generally decreases at part-load, because the process is optimized for design point operation (see Sanz et al., 2005). Decline in efficiency at part-load operation is mainly due to the: (i) increase of heat transfer irreversibilities occuring in the once-through steam generator, (ii) reduced component efficiencies, and (iii) to an increase in heat rejected to the environment relative to loads (Scaccabarozzi et al., 2017). Hereby, strategy S3 achieves clearly better part-load results by attaining a net efficiency of 49.1% at 60% load, compared to 46.7% for strategy S1 and 46.3% for strategy S2. The absolute values for strategy S3 are shown in Table 4. Keeping the TIT constant, as done in control strategy S2 and S3, results in avoidance of larger temperature gradients, especially in the gas turbine system (Snarheim et al., 2005).

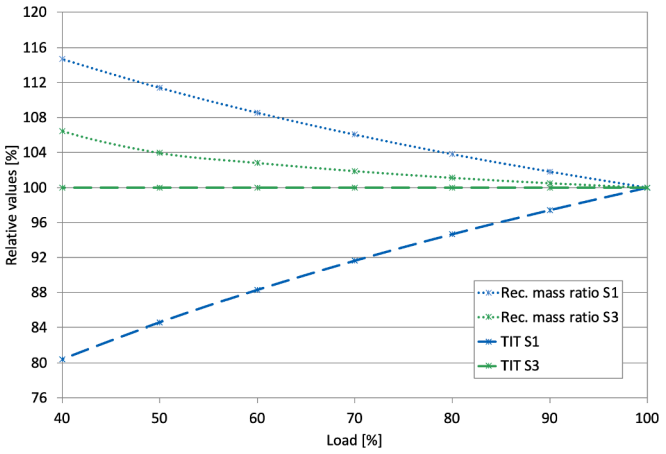

Fig. 10. Comparison between control strategy S1 and S3 in relative values.

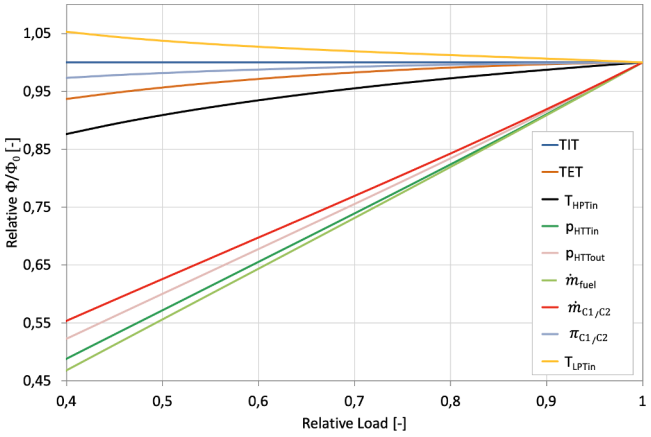

Fig. 12. Relative key process parameters of the Graz Cycle at part-load operation of control strategy 3. *Y*-axis represents relative value of key parameters that are indicated in legend.

4.2. Comparing the control strategies in terms of efficiency

In Figs. 8 and 9, the three strategies are matched in terms of net efficiencies with a single-pressure natural gas combined cycle to portray that the Graz Cycle is effective and comparable to an existing power generating technology. Fig. 8 shows that net efficiency of a combined cycle decreases relatively faster than the applied GC operation modes. In practice, the NGCC features a full-load electrical efficiency of about 58.5%, which declines at reduced loads and reaches at around 50% the "break-even point" with control strategy S3. If loads are reduced further down, the Graz Cycle strategy S3 offers better overall performance (compare Fig. 9). It is worth mentioning, that the NGCC manifests better net efficiencies than control strategy S1 across the total investigated load range. Although strategy S2 shows the worst net efficiency, it is kept in the analysis to indicate that maximum TIT along the load range not automatically results in the overall best performance. Henceforth, control strategy S3 will be discussed due to its highest efficiency. For this purpose, see Table 4 (Appendix B includes tables for control strategy S1 and S2, as well as for the natural gas combined cycle).

First and foremost, the cause of the net efficiency difference will be studied by means of a comparison between strategy S1 and S3. Fig. 10 portaits the differences between control strategy S1 and S3 in terms of recycled mass flow ratio and turbine inlet temperature (TIT). For strategy S1 the TIT decreases rapidly as loads are reduced. In such a way, that at 40% load condition, the temperature is lessened to around 80% of its design value, i.e. $T_0 = 1400$ °C. The recycled mass flow rate constitutes a cooling flow input to the combustion chamber. As the recycled mass flow ratio for control strategy S1 increases at part loads, also the cooling

Table 5
Pros & cons of the discussed control strategies.

Strategy	Pros	Cons
S1		
	• Dynamic response due to throttle control of LPT;	• Non dynamic response of the water stream led to the combustor due to usage of Orifice1.
	• Simplest scheme due to two orifice throttles for HTT cooling;	
	• Lowest investment costs J_c;	
	• Constant CO_2purity at the exhaust gas stream (i.e. above 90%).	
S2		
	• Dynamic response due to throttle control of LPT;	• Highest operational costs J_f because of lowest efficiencies at part loads.
	• Low investment costs J_c;	
	• Constant CO_2 purity at the exhaust gas stream.	
S3		
	• Highest efficiency due to enabled pressure variation in the HRSG and hence higher pressure drop of HTT;	• Low technology readiness level (TRL) of boiler with negative pressure;
	• Optimal economic operation because of high efficiency.	• Relatively high capital costs of vacuum boiler;
		• Slow dynamic response due to floating pressure control of LPT.

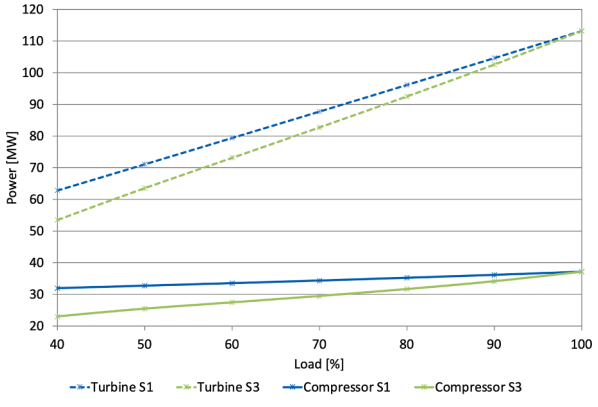

(a) Compression and turbine power for strategy S1 and S3

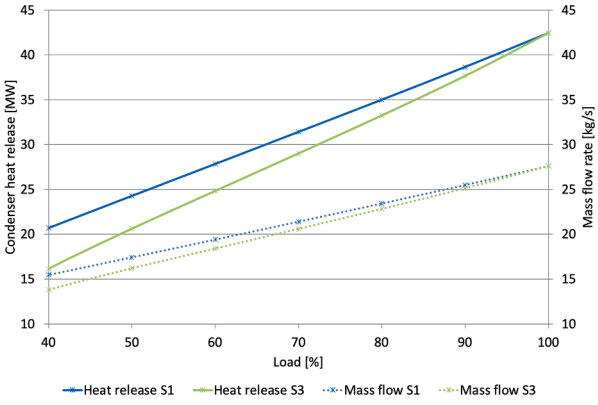

(b) Heat release in the condenser for strategy S1 and S3

Fig. 11. Control strategy S1 vs. S3 at different loads.

effect to the combustor increases, and thus the turbine inlet temperature declines at decreased loads. On the other hand, strategy S3's turbine inlet temperature remains constant, and accordingly the rise of the recycled mass flow ratio in part-load operation is less distinct. The ideal Carnot cycle achieves highest thermodynamic efficiencies by constant elevated heat input into the system as it is replicated by control strategy S3.

Fig. 11a analyses the behaviour of turbine and compressor power at part-load operation for S1 and S3. As already mentioned, for strategy S1 the recycled mass ratio increases as loads diminish. This brings forth reduced cycle mass flow rates in part-load conditions because the fuel input is less. As a result the isentropic efficiencies of the turbomachineries decrease, and since the decline in efficiencies has to be compensated with increasing mass flow rates, the compressor inlet mass flow rate increases due to the necessity of an increase in mass flow of the HTT turbines. As a consequence the compression power in control strategy S1 is almost constant at part-load conditions, whereas the compression power for strategy S3 decreases significantly. This difference in compression power and flow rate trough the compressor stages between S1 and S3 is due to the reduced need of cooling at a constant HTT turbine inlet temperature (i.e. for control strategy S3).

The relation of compression power and the recycled mass flow ratio is shown in Fig. 11a and Fig. 10. Both values are higher in strategy S1. Since the resulting turbine power for strategy S1 also excels the values for strategy S3 at same load conditions (for both control strategies the HTT power accounts for about 85% of the total generated turbine power), the efficiency gain of strategy S3, as stated previously, has to be found elsewhere.

Fig. 11b shows the deviation of the condenser heat release between control strategy S1 and S3. In strategy S1 the heat release in the condenser at 40% load is amounted to 16.3 MW, whereas in strategy S3 the same value is equal to 11.8 MW. That is a difference of 4.5 MW or 28%. This difference stems from the higher mass flow rate through the condenser in S1 (at 40% load 10% more mass flow runs through the condenser). Since the thermal efficiency is linked to the heat output of the system, consequently, the higher heat loss in strategy S1 leads to a lower net plant efficiency compared to strategy S3. If the HRSG pressure is allowed to vary (like it is the case for strategy S3) a greater overall part-load efficiency can be achieved due to the changing pressures on the lower pressure side of the compressors and turbines, so that the pressure ratio of the turbomachinery can be kept almost constant, even when the combustion pressure is reduced.

4.3. Cycle components and system boundaries

A common characteristic of CCS power plants is the heat recovery steam generator, where the heat exchange between the combustion gases and the water/steam occurs. In this component, the hot combustion gases flow - in case of the Graz Cycle - in a counter-current manner trough the shell of the equipment, where the heat exchange with the tube-side water/steam medium takes place in order to produce superheated steam for the steam turbine (Rúa et al., 2020). For this study, a once-through heat recovery steam generator (a single heat exchanger with moving saturation point instead of a configuration with several heat exchangers including a drum and fixed saturation point) is chosen. This is in theory more efficient, because it does not have the necessity of saturation at a fixed location in the exchange progression (Zotică et al., 2020). Since steam generators are bulky equipments, which possess an enormous amount of heat capacity, this leads to a slow response time of the flue gas exiting the HRSG and hence in the power generating LPT.

At the superheater outlet the temperature difference between the two mediums decreases from 15 K at base load to 4 K. Since the OTSG is not a standard component and is designed for design-point (full load) conditions, the low pinch-points in part load are a good side effect regarding the HRSG efficiency. Ideal heat exchange is taken place if the energy transferred per unit temperature is the same in both media at any point, i.e. two counter-flowing parallels in the temperature-heat diagram with a constant ΔT between the lines (Kehlhofer et al., 1999). The losses in an HRSG are often linked with the physical properties of water/steam and the exhaust gas, which do not match. This causes energetic and exergetic losses (Kehlhofer et al., 1999).

Modern gas turbines are often restricted to 40% of its full load power due to combustion instability of the fuel and thereby accruing emissions (Rúa et al., 2020). Referring to Table 4 the gas turbine load has been reduced to roughly 50% of its full potential and is within the limits stated before. However, the Graz Cycle net load is reduced down to 40% in order to ensure stable turndown capacities (i.e. minimum load). For future power generation, this provides and guarantees spinning reserves for the electrical grid as cheap and dispatchable power plants have to run long time periods at low loads (Zaryab et al., 2020).

If we look closer at the fluid properties at 40% part load following is noticed. Since the pressure in the HRSG for control strategy S3 is variable, also the pressures at the exhaust gas drain differ from the 1 bar design point value. It is noteworthy, that the pressure of the stream before entering the CO_2 CPU at 40% reduced load is at 0.5 bar. Considering the compression from 0.5 bar to 1 bar at the exhaust gas drain, would result in 0.6%-points loss in efficiency (i.e. extra power expenditure of 300 kJ for CO_2-compression). This efficiency loss is relative since it depends on where the system boundaries are set. In this study, it is assumed that the CO_2 exit stream enters a partial condensation type of compression and purification unit (CPU), i.e. a "cold box". Indeed, sensitivity analyses of CPUs show that the product pressure does not have a great influence on the energy expenditure (Darde et al., 2009; Lockwood, 2014). Therefore, this efficiency penalty, specifically for control strategy S3, is neglected in the net efficiencies shown in Table 4. The CO_2 stream, fed into a CPU, is processed and compressed to a dense phase, typically around 100 bar (Lockwood, 2014). At this pressure levels, the CO_2 is above its critical point and enters the supercritical fluid phase. There are no common specifications for CO_2 purity delivered by a oxy-combustion power plant to either a pipeline or a storage site (Zheng, 2011). However, a CO_2 recovery $\geq$ 95% can be achieved at the CPU by taking into account that CO_2 purities at GC exhaust gas drain vary between 91% and 87% (in the load range from design conditions to 40% loads for control strategy S3) (Lockwood, 2014). This is also favourable for downstream injection since there is general consensus that the CO_2 concentration should be above 95% (Nord and Bolland, 2020). It is indicated that considering techno-economical aspects discussed in Section 2.1, for this study a "cold box" is found to be favourable. In this scheme, the dried and compressed flue gas is cooled to a very low temperature in order to achieve high CO_2 purities at the outlet (Darde et al., 2009). With decreased CO_2 in the flue gas, a "cold box" is economically more attractive than a CPU scheme without purification. For further details it is referred to (Darde et al., 2009; Lockwood, 2014).

Another phenomenon at this reduced load condition is the decreased C1 compressor inlet temperature from 102.2 °C (i.e. at design point conditions) to 76.4 °C. It is noted, that at this point the steam content of the working fluid enters the first time the wet steam region (i.e. inlet steam quality $x_i < 1$, to wit $x_i = 0.98$). Therefore, load reduction in part-load operation has been limited to 40%, see values in Table 4.

The cooling stream to the HTT turbine increases its mass flow rate in part loads, i.e. the cooling steam mass flow ratio changes occurs from 13.4% at full-load to 22.0% at 40% load. This is due to the decrease in mass flow rates in the turbines at part-load operation, but constant TIT at the HTT inlet section. The cooling of the turbine necessitates indeed less cooling fluid at 40% because of the overall reduced turbine mass troughput, but still enough to keep the turbine blades at a constant temperature (the cooling of the blades takes place by film cooling through holes of the rotating machinery). Besides, for a given cooling technology, the increase in the turbine inlet temperature leads to higher efficiencies, as long as the gain from higher TIT is outbalanced by the various losses caused by the cooling stream (Nord and Bolland, 2020).

4.4. Analysing behaviour of optimal control strategy

Fig. 12 illustrates the performance of control strategy S3, both in full-load and part-load operation down to 40% load (the plot shows relative values of the key parameters). As already mentioned, the turbine inlet temperature is kept constant over the entire load variation at 1400 °C (dark blue line). The HPT inlet temperature is restricted to 600 °C for material reasons, which is not excelled at any point of the load reduction, see also Table 4. The LPT inlet temperature (marked in yellow) is the only process parameter which increases while reducing loads. The reason for this cumulation can be found in decreasing isentropic efficiencies with reduced circulating mass flow rates. This results in a relative increase of the LPT mass flow rate compared to the decrease of the fuel mass flow rate in part-load operation in order to compensate the efficiency loss. The inlet mass flow rate of the LPT turbine is defined by the amount of CO_2 separation, which is controlled by the variable inlet guide vanes of compressor C1.

The outlet pressure of the HTT (equivalent to the hot shell-side pressure of the HRSG) changes from 1.053 (100% load) to 0.55 bar (40%), equal to 0.52 in dimensionless numbers. If this value is allowed to vary (like it is the case for strategy S3), a positive benefit in terms of efficiency is achieved due to the fact that the pressure on the low pressure side of the compressors and turbines is allowed to change. In this case the pressure ratio of the turbomachinery (for instance, the pressure ratio $\pi_{C1/C2}$ of the compressors in light blue) can be kept constant, even when the mass flow is reduced. The reduction of the fuel mass flow rate, signalised by the light green line, declines linearly with relative load. The same is valid for the HTT inlet pressure, which is the pressure at which the combustion process takes place. Therefore, also the oxygen compression expense diminishes constantly, so that the same specific energy consumption is maintained when operating at part-load conditions.

4.5. Dynamic operation

Natural gas oxy-combustion cycles manifest two different dynamic operation patterns. Firstly, the gas turbines react very quickly by changing their operation point within a few seconds and have therefore negligible dynamics (Rúa and Nord, 2020). Secondly, the heat recovery steam generator exhibit in opposite a dominant dynamic behaviour and limits the transient operation of the steam cycle. The large storage capacity of this relatively bulk component leads to operational time lags of 10 to 20 min, depending on the size of the power plant, and represents thereby the bottleneck during dynamic operation of thermal power plants (Alobaid et al., 2017; Rúa and Nord, 2020). In natural gas combined cycles (NGCC), the gas turbine drives the transient operation and the steam cycle sets the timeframe to reach steady-state operation (Rúa et al., 2020). This slow dynamic response of the water steam cycle, however, does not effect the power generation flexibility of the asset since gas turbines can over- and under-shoot in order to balance the slow dynamics, leading thereby to strained power control (Rúa and Nord, 2020).

5. Discussion and conclusions

Large fluctuations in demand and volatile renewable energies require quick reactions from power plants in order to keep the balance between supply and demand. Herein lies the fundamental importance of CCS power plants and in particular in this study. Especially, gas turbine power plants and hydro power stations can react rapidly on load changes. In the timeframe of 15 minutes they can start-up and reach the full load, whilst a combined cycle power plant in the same time frame reaches only half of its installed capacity. In comparison coal and nuclear power plants ramp very slowly, since they take somewhat like 36 hours to reach their full load (IEA, 2011). Indeed, part-load and transient operation (load changes and start-up) will grow in significance for thermal power plants. In this context and as evidenced in this research paper, the oxy-combustion Graz Cycle promises to have better part-load efficiencies than a state-of-the-art single pressure combined cycle plant at a part-load condition of 50% load or less. This is due to its elevated integrated and mass recycled nature. Moreover, the Graz Cycle is not only a net-zero emission power plant but features very high efficiencies at full-load operation (net plant efficiency of 53.1%). Latter results show that the Graz Cycle can be easily named alongside the well researched Allam cycle (Chan et al., 2021; Haseli and Sifat, 2021; Scaccabarozzi et al., 2017; Wimmer and Sanz, 2020; Yu et al., 2021; Zaryab et al., 2020). For instance, the part-load results of control strategy S3 are listed in Table 4. More about the integration of the Graz Cycle in the future power grid is detailed in Appendix A.

In this study, control strategies for the Graz Cycle are developed and part-load simulations are performed to enhance its operational flexibility and to assure high efficiencies. The determination of a control strategy is generally crucial for the day-to-day operation of a power plant, and furthermore the assessment of different control strategies leads to different efficiencies due to different operational modes in part loads and is relevant for transient operation, such as load changes. Dynamic simulations of a power plant can only be performed upon an existing control operation mode. The control strategy for gas turbine cycles and combined cycles is very well analysed in standard literature (Gülen, 2019; Kehlhofer et al., 1999) and pros and cons are understood. In contrast, for oxy-combustion CCS cycles, which have often interlaced cycle schemes, the right control strategy is uniquely important.

An important aspect of this work is the controllability of the GC. For this purpose different suitable control strategies are studied and implemented into the simulation in order to meet the requirements of the power cycle in the most efficient way. More precisely, a systematic framework is chosen in order to evaluate manipulated and controlled variables. The operation of the Graz Cycle is analysed in a top-down analysis differing between primary control and secondary control loops. The most efficient control strategy (S3) has following asset: the pressure in the heat recovery steam generator, for instance a once-through boiler, is allowed to vary (i.e. the pressure is floating), the turbine inlet temperature remains on a maximum value and loads are reduced down to 40% with favourable results, i.e. a 44.7% net plant efficiency at this load condition.

To sum up, following relations are in force for the efficiencies of the three investigated control strategies:

$$\eta_{S3} \gg \eta_{S1} > \eta_{S2},$$

and accordingly the fixed operational costs J_f for S1, S2 and S3 are:

$$J_{f_{S3}} \ll J_{f_{S1}} < J_{f_{S2}}.$$

On the other hand, the total capital costs J_c penalise control strategy S3 because the boiler is operated below atmospheric pressures and thus necessitates more on investment costs. Pros and cons of the different operation modes are summarised in Table 5 by analysing specific parameters, such as efficiency, costs and dynamic response of the operating system.

Of interest for future work in order to complement this study is:

- An investigation comprising realistic behaviours of the part-load efficiency of the compressors featuring variable inlet guide vanes and including more detailed compressor maps;
- A research on the dynamic behaviour of the cycle components in order to be able to predict transient operation and load changes;
- A closed-cycle model consisting of dynamic models that allows a detailed assessment of its simultaneous transient operation under different load points;
- A study of start-up and shut-down strategies for the Graz Cycle;

- A further work to treat carbon dioxide removal (CDR) by combining the Graz Cycle with biomass products (i.e. syngas) in order to achieve negative emissions.

CRediT authorship contribution statement

Benjamin Mitterrutzner: Conceptualization, Methodology, Software, Investigation, Writing – original draft, Writing – review & editing, Visualization. **Wolfgang Sanz:** Conceptualization, Writing – review & editing, Supervision. **Lars O. Nord:** Conceptualization, Methodology, Writing – review & editing, Supervision.

Declaration of Competing Interest

The authors declare that they have no known competing financial interests or personal relationships that could have appeared to influence the work reported in this paper.

Acknowledgements

Benjamin Mitterrutzner would like to thank his two supervisors Wolfgang Sanz and Lars O. Nord for their patience and always valuable advices. He emphasizes that great part of this study has been completed during his master's thesis project. Moreover, he would like to thank Ruben Mocholi Montanes and Rohan Dutta for their kind support during his stay at NTNU. This research abroad project was kindly supported by Graz University of Technology within the exchange program "KUWI".

Appendix A. Additional context regarding integration of CCS into existing power grid

In the following paragraphs a brief overview of the possibilities of integration of CCS power plants into the existing power grid is given that were omitted from the main body. In particular, it is aimed at providing information about synergy effects of implementation of oxy-combustion power plants (e.g. Graz Cycle) in the future electricity sector. To better contextualise this study it is pointed towards operational strategies of this CCS power plant, not only emphasising the necessity of part-load operation, as it is already explained well enough in the introduction.

The future energy system will be deeply penetrated by renewable energy sources, especially solar and wind energies, also due to boundaries and limited quantities of fossil fuel resources (Bruckner et al., 2014; IEA, 2021). Moreover, the energy mix in 2050 and beyond will be way more diverse than today (IEA, 2021). However, there are a few constraints which limit the deployment of intermittent renewable energy sources (IRES) on a large scale (Bui et al., 2018):

(i) IRES do not provide firm capacity due to its volatile input and therefore fluctuating output, nor do they allocate ancillary services like frequency response or reserve capacity;
(ii) Their intermittent nature demand more of ancillary services from the electrical grid in order to overcome peaks and spikes such as e.g. conventional power plants;
(iii) Correlated nature of wind and solar energies leads to energy system methods, where highest production of renewables does not coincide with current electricity demand.

Above mentioned reasons do make the introduction of CCS in power generation necessary not only on a cost (Gross et al., 2012) and on a emission abating level (Pachauri et al., 2014) but to provide balancing services to the grid (i.e. in form of frequency response, reserve and inertial services) Bui et al. (2018). Recent studies (Bui et al., 2018; Hanak and Manovic, 2020) have emphasized, that CCS plants have some additional advantages (over unabated plants), specifically to store energy over time by shifting energy intensive processes, such as the separation of oxygen in the air separation unit of an oxy-combustion power plant. This requires electricity for air compression (charging mode), which could then be released in the discharging mode whilst the power plant is operating. The charging mode could be scheduled at times of excess power *via* renewables and provide reserves and frequency responses, to wit act as a buffer (see Fig. A.13). From techno-economical point of view this operation strategy makes a lot of sense, since during times of low energy demand, the air separation unit could be kept in charging mode (i.e. the oxygen becomes liquefied and stored on site). During peak energy demans this store could than be subsequently used as cheap oxygen supply to the combustor by lowering the operational costs (Lockwood, 2014).

To sum up, the main advantages of an oxy-combustion CCS power plant are:

- Zero CO_2 and NO_x emissions (Fernandes et al., 2019)
- High full-load and part-load efficiency
- High flexibility in operation and design
- Potential for energy storage (Lockwood, 2014; Perrin et al., 2015)
- A "non-chemical" route (Perrin et al., 2015)

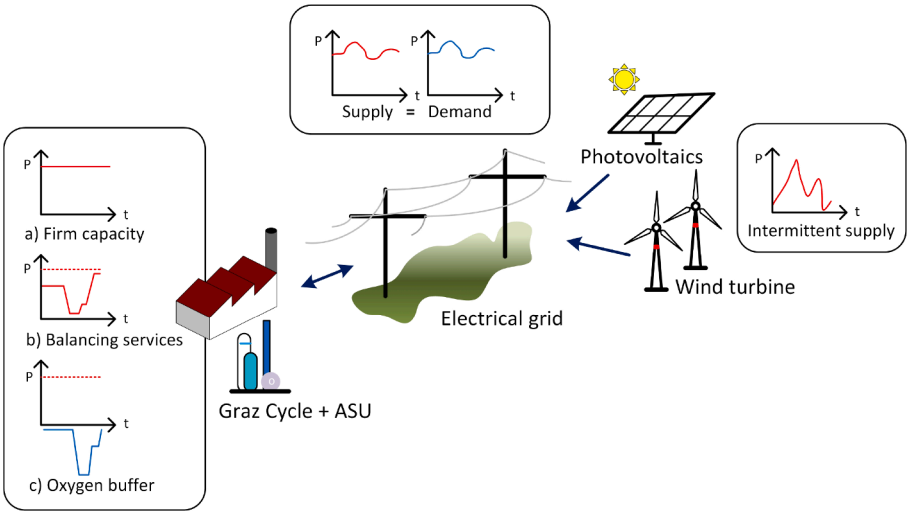

Fig. A1. Integration of CCS into the future electricity system.

Appendix B. Summary tables

Table B.6 show the key variables and performance results of the single-pressure natural gas combined cycle.

Table B.7 and B.8 summarises the key data of part-load performance for control strategy S1 and S2, respectively.

Table B1
Key performance results of the single-pressure NGCC with the same turbomachinery specifications as applied for the Graz power cycle. The combined cycle conserves a high maximum turbine inlet temperature down to ~50% load.

Net overall load [%]	100	90	80	70	60	50	40
Net cycle efficiency (incl. losses) [%]	58.46	56.92	54.97	52.67	50.02	46.95	43.32
Gas turbine inlet temperature [°C]	1400.0	1338.3	1274.5	1208.7	1139.8	1066.3	987.1
Gas turbine outlet temperature [°C]	654.4	618.8	582.1	544.4	505.1	463.3	418.6
Gas turbine inlet pressure [bar]	25.0	24.5	24.0	23.4	22.8	22.2	21.5
Stack exhaust gas temperature [°C]	121.8	138.2	152.2	164.0	173.8	181.7	187.3
Stack exhaust gas pressure [bar]	1.013	1.013	1.013	1.013	1.013	1.013	1.013
Condenser pressure [bar]	0.041	0.041	0.041	0.041	0.041	0.041	0.041
Approach temperature [K]	7.0	7.0	7.0	7.0	7.0	7.0	7.0
Minimum temperature difference in the HRSG [K]	8.0	7.6	7.0	6.3	5.7	5.0	4.2
Live-steam pressure [bar]	104.1	93.1	82.5	72.3	62.3	52.3	42.4
Live-steam temperature [°C]	586.2	570.0	549.1	523.8	493.6	458.1	416.9

Table B2
Key performance data of the Graz Cycle with CO_2 capture for control strategy S1.

Net overall load [%]	This study						
	100	90	80	70	60	50	40
Thermal cycle efficiency [%]	66.3	65.1	63.7	61.9	59.7	56.8	53.0
Net electrical cycle efficiency (incl. losses) [%]	64.4	63.3	61.9	60.2	58.00	55.2	51.5
Efficiency considering O_2-supply [%]	55.1	54.0	52.6	50.9	48.7	45.9	42.1
Net efficiency (incl. CO_2-compression) [%]	53.1	52.0	50.6	48.9	46.7	43.9	40.2
HTT power [MW]	95.50	88.29	81.23	74.28	67.38	60.55	53.76
Total turbine power [MW]	113.23	104.66	96.17	87.76	79.41	71.10	62.81
Total compression power [MW]	37.12	36.12	35.20	34.33	33.51	32.71	31.93
Electrical power output (incl. losses) [MW]	73.45	66.10	58.76	51.41	44.07	36.72	29.38
O_2generation and compression [MW]	10.64	9.74	8.85	7.96	6.85	5.91	4.98
CO_2compression to 100 bar [MW]	2.19	2.01	1.82	1.64	1.46	1.28	1.10
Net power output [MW]	60.62	54.36	48.09	41.81	35.53	29.25	22.96
Total heat input [MW]	113.75	104.15	94.66	85.22	75.79	66.38	56.94
CO_2-purity at the exhaust gas drain [%]	90.5	90.5	90.5	90.5	90.5	90.4	90.2
HTT inlet temperature [°C]	1400.0	1364.0	1325.3	1282.9	1236.2	1184.2	1125.7
HTT exhaust gas temperature [°C]	568.8	556.9	543.5	528.2	510.7	490.4	466.6
HTT inlet pressure [bar]	40.0	37.8	35.6	33.35	31.1	28.9	26.6
HTT outlet pressure [bar]	1.053	1.053	1.053	1.053	1.053	1.053	1.053
HPT inlet temperature [°C]	554.1	540.6	525.0	506.6	484.7	458.2	425.6
HPT inlet pressure [bar]	185.1	173.8	162.4	150.9	139.1	126.9	114.3
LPT inlet temperature [°C]	203.1	211.3	219.9	229.0	238.9	249.6	261.4
LPT outlet pressure [bar]	0.041	0.041	0.041	0.041	0.041	0.041	0.041
C1/C2 pressure ratio [–]	41.2	39.0	36.8	34.6	32.4	30.2	27.9
C1 inlet temperature [°C]	102.2	112.3	122.7	133.5	144.8	156.7	169.1
Minimum temperature difference in the HRSG [°C]	5.0	4.7	4.4	4.0	3.7	3.4	3.1
Cooling steam mass flow ratio [%]	13.4	13.2	13.1	12.9	12.8	12.5	12.3
Recycled stream mass flow ratio [%]	53.7	54.6	55.7	56.9	58.2	59.8	61.5

Table B3
Key performance data of the Graz Cycle with CO_2 capture for control strategy S2.

Net overall load [%]	This study				
	100	90	80	70	60
Thermal cycle efficiency [%]	66.3	65.0	63.5	61.6	59.3
Net electrical cycle efficiency (incl. losses) [%]	64.4	63.2	61.7	59.8	57.6
Efficiency considering O_2-supply [%]	55.1	53.9	52.4	50.5	48.3
Net efficiency (incl. CO_2-compression) [%]	53.1	51.9	50.4	48.6	46.3
HTT power [MW]	95.49	87.80	80.23	72.71	65.19
Total turbine power [MW]	113.23	104.42	95.67	86.94	78.25
Total compression power [MW]	37.11	35.88	34.70	33.53	32.36
Electrical power output (incl. losses) [MW]	73.45	66.10	58.76	51.41	44.07
O_2generation and compression [MW]	10.64	9.76	8.88	8.01	7.13
CO_2compression to 100 bar [MW]	2.19	2.01	1.83	1.65	1.47
Net power output [MW]	60.62	54.34	48.05	41.76	35.47
Total heat input [MW]	113.75	104.34	95.01	85.69	76.32
CO_2-purity at the exhaust gas drain [%]	90.5	90.5	90.5	90.5	90.5
HTT inlet temperature [°C]	1400.0	1400.0	1400.0	1400.0	1400.0
HTT exhaust gas temperature [°C]	568.8	558.2	546.2	532.4	516.0
HTT inlet pressure [bar]	40.0	37.0	34.0	31.0	28.0
HTT outlet pressure [bar]	1.053	1.053	1.053	1.053	1.053
HPT inlet temperature [°C]	554.1	542.0	527.8	511.1	490.7
HPT inlet pressure [bar]	185.1	174.4	163.7	152.6	141.0
LPT inlet temperature [°C]	203.1	210.5	218.2	226.8	236.3
LPT outlet pressure [bar]	0.041	0.041	0.041	0.041	0.041
C1/C2 pressure ratio [–]	41.2	38.2	35.2	32.3	29.3
C1 inlet temperature [°C]	102.2	111.0	120.1	130.0	140.7
Minimum temperature difference in the HRSG [°C]	5.0	4.7	4.4	4.1	3.8
Cooling steam mass flow ratio [%]	13.4	17.4	21.9	27.2	33.3
Recycled stream mass flow ratio [%]	53.7	54.6	55.7	56.9	58.2

References

Alobaid, F., Mertens, N., Starkloff, R., Lanz, T., Heinze, C., Epple, B., 2017. Progress in dynamic simulation of thermal power plants. Prog. Energy Combust. Sci. 59, 79–162.

Boyce, M.P., 2002. Handbook for Cogeneration and Combined Cycle Power Plants. ASME Press.ISBN: 0-7918-0169-1.

Boyce, M.P., 2011. Gas Turbine Engineering Handbook. Elsevier.ISBN: 0123838428.

Bruckner, T., Bashmakov, I. A., Mulugetta, Y., Chum, H., De la Vega Navarro, A., Edmonds, J., Faaij, A., Fungtammasan, B., Garg, A., Hertwich, E., et al., 2014. Energy systems.

Bui, M., Adjiman, C.S., Bardow, A., Anthony, E.J., Boston, A., Brown, S., Fennell, P.S., Fuss, S., Galindo, A., Hackett, L.A., et al., 2018. Carbon capture and storage (CCS): the way forward. Energy Environ. Sci. 11 (5), 1062–1176.

Center for Climate and Energy Solutions, 2017. "Global Manmade Greenhouse Gas Emissions by Sector, 2013".

Chan, W., Li, H., Li, X., Chang, F., Wang, L., Feng, Z., 2021. Exergoeconomic analysis and optimization of the Allam cycle with liquefied natural gas cold exergy utilization. Energy Convers. Manag. 235, 113972.

Darde, A., Prabhakar, R., Tranier, J.-P., Perrin, N., 2009. Air separation and flue gas compression and purification units for oxy-coal combustion systems. Energy Procedia 1 (1), 527–534.

European Commission, 2011. Energy roadmap 2050.

Fan, K., Yang, C., Xie, Z., Ma, X., 2021. Load-regulation characteristics of gas turbine combined cycle power system controlled with compressor inlet air heating. Appl. Therm. Eng. 196, 117285.

Fernandes, D., Wang, S., Xu, Q., Chen, D., 2019. Dynamic simulations of the Allam cycle power plant integrated with an air separation unit. Int. J. Chem. Eng. 10. https://doi.org/10.1155/2019/6035856. Article ID 6035856.

Fischedick, M., Görner, K., Thomeczek, M., 2015. CO_2: Abtrennung, Speicherung, Nutzung: Ganzheitliche Bewertung im Bereich von Energiewirtschaft und Industrie. Springer-Verlag.ISBN: 978-3-642-19527-3.

Gross, R., Heptonstall, P., Leach, M., Skea, J., Anderson, D., Green, T., 2012. The UK energy research centre review of the costs and impacts of intermittency. Renewable Electricity and the Grid: The Challenge of Variability, p. 73.

Gülen, S.C., 2019. Gas Turbines for Electric Power Generation. Cambridge University Press.ISBN: 9780367199579.

Hanak, D.P., Manovic, V., 2020. Linking renewables and fossil fuels with carbon capture via energy storage for a sustainable energy future. Front. Chem. Sci. Eng. 14 (3), 453–459. https://doi.org/10.1007/s11705-019-1892-2.

Haseli, Y., Sifat, N., 2021. Performance modeling of Allam cycle integrated with a cryogenic air separation process. Comput. Chem. Eng. 148, 107263.

IEA, 2011. Harnessing Variable Renewables - A Guide to the Balancing Challenge. chapter Introduction. p. 25.

IEA, 2020. "Global CO_2 emissions by sector, 2018".

IEA, 2021. "Net Zero by 2050: A Roadmap for the Global Energy Sector, 2021".

IEAGHG, 2015. Oxy-combustion turbine power plants.

Imsland, L., Snarheim, D., Ulfsnes, R., Bolland, O., Foss, B.A., 2004. Modeling and control of a O_2/CO_2 gas turbine cycle for CO_2 capture. IFAC Proc. Vol. 37 (9), 727–732.

Johnsson, F., Odenberger, M., Göransson, L., 2013. Challenges to Integrate CCS into Low Carbon Electricity Markets. Elsevier.

Jordal, K., Bolland, O., Klang, A., 2003. Aspects of cooled gas turbine modelling for the semi-closed O_2/CO_2 cycle with CO_2 capture. Turbo Expo: Power for Land, Sea, and Air, 3686, pp. 53–64.

Jüdes, M., Vigerske, S., Tsatsaronis, G., 2009. Optimization of the design and partial-load operation of power plants using mixed-integer nonlinear programming. Optimization in the Energy Industry. Springer, pp. 193–220.

Kehlhofer, R., Hannemann, F., Rukes, B., Stirnimann, F., 2009. Combined-Cycle Gas & Steam Turbine Power Plants, third ed. Pennwell Books.ISBN: 978-1-59370-168-0.

Kehlhofer, R., Warner, J., Nielsen, H., Bachmann, R., 1999. Combined-Cycle Gas & Steam Turbine Power Plants, second ed. PennWell.ISBN: 9780878147366.

Koohestanian, E., Shahraki, F., 2021. Review on principles, recent progress, and future challenges for oxy-fuel combustion CO_2 capture using compression and purification unit. J. Environ. Chem. Eng. 9 (4), 105777. https://doi.org/10.1016/j.jece.2021.105777. ISSN 2213-3437.

Lechner, C., Seume, J., 2018. Stationäre Gasturbinen. Springer-Verlag.ISSN: 2512–5281.

Littlecott, C., Scott, V., Haszeldine, S., 2014. Carbon Capture and Storage in the EUs 2030 Climate and Energy Framework. Technical Report. SCCS Policy Briefing.

Lockwood, T., 2014. Developments in oxyfuel combustion of coal. IEA Clean Coal Centre 300, 240.

Mehrpanahi, A., Payganeh, G., 2017. Multi-objective optimization of IGV position in a heavy-duty gas turbine on part-load performance. Appl. Therm. Eng. 125, 1478–1489.

Metz, B., Davidson, O., De Coninck, H., et al., 2005. Carbon Dioxide Capture and Storage: Special Report of the Intergovernmental Panel on Climate Change. Cambridge University Press.ISBN: 9780521866439.

Milewski, J., Badyda, K., Miller, A., 2012. Gas turbines in unconventional applications. Efficiency, Performance and Robustness of Gas Turbines, p. 121.

Miller, A., Lewandowski, J., Badyda, K., Kiryk, S., Milewski, J., Hama, J., Iki, N., 2003. Off-design analysis of the GRAZ Cycle performance. Proceeding of the International Gas Turbine Congress 2003, Tokyo, November 2–7.

Mitterrutzner, B., 2020. Process Simulation of the Graz Power Cycle. Graz University of Technology / Norwegian University of Science and Technology. Master's thesis. https://diglib.tugraz.at/download.php?id=60a4e9fca1728&location=browse.

Montanes, R.M., 2018. Transient Performance of Combined Cycle Power Plant with Absorption Based Post-combustion CO_2 Capture: Dynamic Simulations and Pilot Plant Testing. Norwegian University of Science and Technology. Ph.D. thesis.

Moon, S.W., Kim, T.S., 2020. Advanced gas turbine control logic using black box models for enhancing operational flexibility and stability. Energies 13 (21), 5703.

Nord, L.O., 2010. Pre-combustion CO_2 Capture: Analysis of Integrated Reforming Combined Cycle. Norwegian University of Science and Technology. Ph.D. thesis.

Nord, L.O., Bolland, O., 2020. Carbon Dioxide Emission Management in Power Generation. John Wiley & Sons.ISBN: 9783527347537.

Pachauri, R.K., Allen, M.R., Barros, V.R., Broome, J., Cramer, W., Christ, R., Church, J.A., Clarke, L., Dahe, Q., Dasgupta, P., et al., 2014. Climate change 2014: synthesis report. Contribution of Working Groups I, II and III to the Fifth Assessment Report of the Intergovernmental Panel on Climate Change. IPCC.

Perrin, N., Dubettier, R., Lockwood, F., Tranier, J.-P., Bourhy-Weber, C., Terrien, P., 2015. Oxycombustion for coal power plants: advantages, solutions and projects. Appl. Therm. Eng. 74, 75–82.

Prosser, N., Shah, M., 2011. Air separation units for oxy-coal power plants. 2nd Oxyfuel Combustion Conference, pp. 12–16.

Rúa, J., Bui, M., Nord, L.O., Mac Dowell, N., 2020. Does CCS reduce power generation flexibility? A dynamic study of combined cycles with post-combustion CO_2 capture. Int. J. Greenh. Gas Control 95, 102984.

Rúa, J., Nord, L.O., 2020. Optimal control of flexible natural gas combined cycles with stress monitoring: linear vs. nonlinear model predictive control. Appl. Energy 265, 114820.

Sanz, W., Braun, M., Jericha, H., Platzer, M.F., 2018. Adapting the zero-emission Graz Cycle for hydrogen combustion and investigation of its part load behavior. Int. J. Hydrog. Energy 43 (11), 5737–5746.

Sanz, W., Jericha, H., Luckel, F., Göttlich, E., Heitmeir, F., 2005. A further step towards a Graz Cycle power plant for CO_2 capture. ASME Paper GT2005-68456.

Sanz, W., Jericha, H., Moser, M., Heitmeir, F., 2004. Thermodynamic and economic investigation of an improved Graz cycle power plant for CO_2 capture. Turbo Expo: Power for Land, Sea, and Air, 41723, pp. 409–418.

Scaccabarozzi, R., Gatti, M., Martelli, E., 2017. Thermodynamic optimization and part-load analysis of the NET power cycle. Energy Procedia 114, 551–560.

Seborg, D.E., Edgar, T.F., Mellichamp, D.A., Wiley, H., 2008. Process dynamics and control, second ed. ISBN: 0-471-00077-9.
SimTech Simulation Technology, 2017. "IPSEpro Overview".
Sinnott, R., 2005. Chemical Engineering Design In: Coulson and Richardsons Chemical Engineering Series, fourth ed., 6. Elsevier Butterworth-Heinemann.ISBN: 9780080418650.
Skogestad, S., 2004. Control structure design for complete chemical plants. Comput. Chem. Eng. 28 (1–2), 219–234.
Snarheim, D., Imsland, L., Foss, B.A., Ulfsnes, R., Bolland, O., 2005. Control design for a gas turbine cycle with CO_2 capture capabilities. IFAC Proc. Vol. 38 (1), 109–114.
Stodala, A., Die Dampfturbinen, 1910. ISBN: 978-3-642-90437-0.
Ulfsnes, R.E., Bolland, O., Jordal, K., 2003. Modelling and simulation of transient performance of the semi-closed O_2/CO_2 gas turbine cycle for CO_2-capture. ASME Turbo Expo 2003, Collocated with the 2003 International Joint Power Generation Conference. American Society of Mechanical Engineers Digital Collection, pp. 65–74.
Wimmer, K., Sanz, W., 2020. Optimization and comparison of the two promising oxy-combustion cycles NET power cycle and Graz Cycle. Int. J. Greenh. Gas Control 99, 103055.
Yu, H., Gundersen, T., Gençer, E., 2021. Optimal liquified natural gas (LNG) cold energy utilization in an Allam cycle power plant with carbon capture and storage. Energy Convers. Manag. 228, 113725.
Zaryab, S.A., Scaccabarozzi, R., Martelli, E., 2020. Advanced part-load control strategies for the Allam cycle. Appl. Therm. Eng. 168, 114822.
Zero Emissions Platform, 2013. CO_2 Capture and Storage - Recommendations for Transitional Measures to Drive Deployment in Europe. Technical Report. European Commission.
Zheng, L., 2011. Oxy-Fuel Combustion for Power Generation and Carbon Dioxide (CO_2) Capture. Elsevier.ISBN: 978-1-84569-671-9.
Zotică, C., Nord, L.O., Kovacs, J., Skogestad, S., 2019. Optimal operation and control of heat-to-power cycles: a new perspective using a systematic plantwide control approach. Computer Aided Chemical Engineering, 46. Elsevier, pp. 1429–1434.
Zotică, C., Nord, L.O., Kovács, J., Skogestad, S., 2020. Optimal operation and control of heat to power cycles: a new perspective from a systematic plantwide control approach. Comput. Chem. Eng. 141, 106995.